5.3 Seismological Studies of the Deformation of Oceanic Lithosphere

Seth Stein and Emile A. Okal

Department of Geological Sciences, Northwestern University, Evanston, Illinois, USA

I. Introduction

Global earthquake seismology and plate tectonics have developed in a parallel and closely coupled manner during the last 20 years. Seismological instrumentation and techniques evolve sufficiently rapidly that seismology continues to provide new insight on tectonic questions of current interest.

During the first decade of plate tectonics, 1965–1975, many investigations focused on present-day plate *kinematics*, defining the location and nature of motion on plate boundaries. Introduction of the World Wide Standardized Seismograph Network in 1963 provided reliable earthquake locations

SPACE GEODESY AND GEODYNAMICS
ISBN 0-12-057840-9

which helped delineate mid-ocean ridge systems and downgoing plates at subduction zones. The large dataset that was obtained from reliably calibrated seismic stations with adequate global distribution yielded earthquake focal mechanisms demonstrating extension at spreading centers, subduction at convergent boundaries and confirming the predicted strike-slip motion on transform faults (an adequate listing of the relevant papers would involve several hundred; see Cox (1973) for a review). The geometry of earthquake mechanisms, along with spreading rates from magnetic anomalies and transform azimuths, formed the basis for models of global relative plate motions (Chase, 1978; Minster and Jordan, 1978).

With the general kinematics of present plate motions established, increasing attention has been devoted to three general issues:

(i) dynamics of plate tectonic processes,
(ii) deformation within plates, and
(iii) evolution of plate boundaries.

These topics are coupled and cannot be discussed separately: for example, intraplate deformation often reflects either forces applied to plates or plate boundary evolution. As these questions came to the fore, by about 1975, new methods in seismology provided important insights. The purpose of this chapter is to briefly review some of these results for a nonseismological audience. We first illustrate some seismological techniques, and then discuss plate scale processes, plate boundary processes and localized intraplate processes. Due to length limitations, we restrict our attention to the oceanic lithosphere.

II. Techniques

The before mentioned results were obtained by analyzing most exclusively the polarity (or direction of motion) of the first arrival ("*P*" wave) on seismic records; following advances in theoretical seismology, newer methods now allow general use of longer portions of the waveform. While their goal remains the traditional one of determining earthquake depth, fault orientation and direction and history of slip (Fig. 1), these techniques provide considerably better resolution than was previously possible.

The first method, *body wave modeling*, matches the first minute or two of the *P*-wave seismogram. This approach uses an algorithm which computes the seismogram as a sum of the direct P wave and of near-surface reflections and conversions (Fukao, 1970; Langston and Helmberger, 1975; Kroeger and Geller, 1986). The radiation pattern of the earthquake source, reflection coefficients at interfaces and the delay of the different reflections are included. The resulting series of impulses with the correct amplitudes and

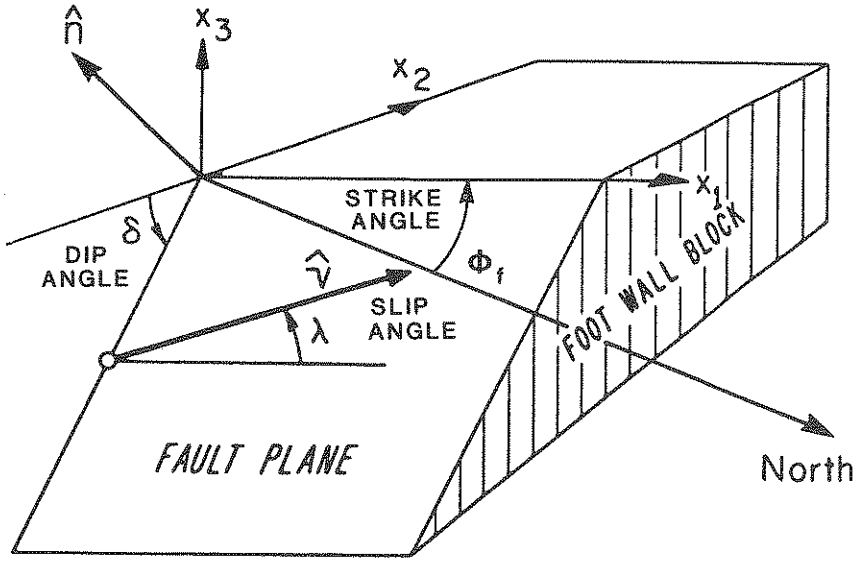

Fig. 1. Fault geometry used in seismological studies. The fault is treated as planar and characterized by strike ϕ, dip δ, and slip λ angles.

delays is convolved with operators representing the pulse generated by the earthquake (source time function), attenuation along the ray path and the seismometer transfer function (Fig. 2). Synthetic seismograms are generated for a range of possible parameters and the best fit to the data found by direct matching or a formal error criterion.

This method defines a best-fitting fault geometry consistent with first motion data, and constrains both focal depth and source time function. It is especially useful for constraining focal depth from the delay of the free surface reflections pP and sP, and of the water bottom reflection pwP, relative to the direct P pulse (Fig. 2). P waveforms also depend on source parameters other than depth; fortunately, the time separation between arrivals, which provides most of the depth information, is relatively insensitive to focal mechanism and source time function. The accuracy of depth estimates relying on travel-time data alone can be as poor as 30 km, especially in remote oceanic locations with no regional station coverage; while they correctly define the brittle lithosphere as a shallow layer (e.g. in a subducting plate), such estimates cannot resolve earthquake depths within the lithosphere. Thus body wave modeling, with depth resolution of several kilometers, proves very valuable for tectonic studies. The depth defined by this process is known as the centroid depth, the average depth of a fault surface which may extend over some depth range.

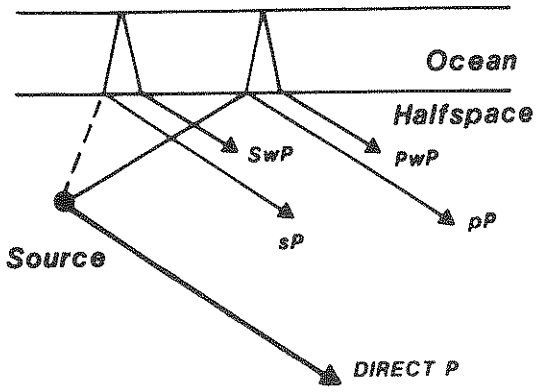

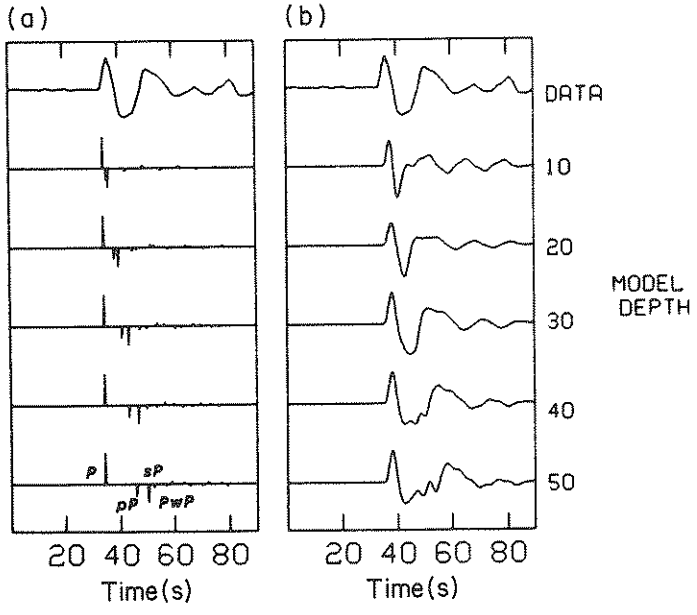

STRIKE 256 DIP 67 SLIP 128 TIME FUNCTION 1,1.5,1

Fig. 2. Body-wave modeling procedure for depth determination. (a) Synthetic seismograms for an assumed fault geometry and (b) including the effects of the seismometer and attenuation calculated for various depths. The data are best fit by a depth near 30 km.

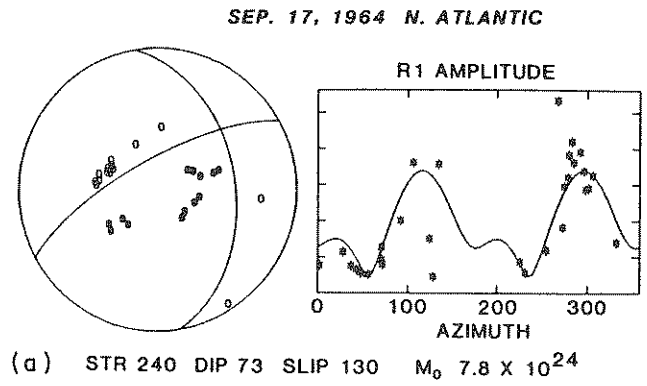

Fig. 3. Surface wave focal mechanism study for (a) thrust, (b) normal, and (c) strike–slip fault arthquakes. The theoretical Rayleigh wave amplitude radiation patterns shown yield the best t to the data consistent with the first motions (Wiens and Stein, 1984).

Analogous techniques derive information from the waveforms of *surface waves.* The theory of the Earth's normal modes allows theoretical waveforms to be computed for an assumed fault geometry, depth, source time function and Earth structure model (Aki and Richards, 1980). This process is easier to visualize in the frequency domain by considering the wave's radiation pattern; Fig. 3 shows spectral amplitude (smooth curves) as a function of azimuth for several different fault geometries; phase radiation patterns can be similarly computed. The data (asterisks) are derived by correcting spectral amplitudes on seismograms at different distances and azimuths from the earthquake to a common distance. This process removes the amplitude effects of attenuation and geometrical spreading and the phase effect of propagation. The corrected (equalized) data are compared to theoretical spectra for fault geometries satisfying the first motion data (Fig. 3), yielding reliable mechanisms when first motion data alone do not constrain the solution. Since radiation patterns depend on focal depth, depth can be estimated by modeling at various depths and identifying the best fit.

The primary limitation of this method results from the variation in velocity structure with position on the Earth. If not correctly included when equalizing to a common distance, this effect results in apparent noise, especially for phase data. Since longer-period waves "integrate" Earth structure over longer wavelengths, this effect is most significant at short periods, but becomes substantial at long periods for waves having circled the Earth several times. Efforts are being made to incorporate the influence of such *lateral heterogeneity* in surface wave analyses.

Both surface- and body-wave modeling suffer from the fact that the observed seismogram depends nonlinearly on the fault strike, dip and slip angles. It is thus difficult to formally invert data for a best fitting solution. This difficulty can be surmounted by using a moment tensor representation which describes the source as a set of forces and force couples. The moment tensor has two advantages: the seismogram is linear in its elements and can thus be inverted and the tensor represents sources more general than slip on a planar fault (for example, an opening crack) (Aki and Richards, 1980). Moment tensor inversion of surface wave data is conducted for an assumed depth, which can be varied for a best fit. Inclusion of lateral heterogeneity in velocity improves the inversion results.

III. Plate-wide Processes

A. Earthquake Depths and Rheology of the Lithosphere

The thickness of the lithosphere, the upper layer of strong material which deepens as the plate cools, has been inferred from several techniques wit

different results. The differences result primarily, as discussed later, from the different characteristic times of the forces applied to the plates. *Seismic thickness*, the depth to the low-velocity zone, is measured from surface wave dispersion studies (Forsyth, 1975; Yu and Mitchell, 1979); *elastic thickness*, estimated from flexure below mid-plate loads (Bodine *et al.*, 1981), is found to be much less than seismic thickness. The depths of oceanic intraplate earthquakes provide another measure as the maximum depth of seismicity increases with lithospheric age. Comparison with predicted thermal structures (Fig. 4) indicates that the maximum depth of seismicity corresponds approximately to the 750°C isotherm (Chen and Molnar, 1983; Wiens and Stein, 1983, 1984). The thickness of the seismically active portion of the lithosphere is equal to or slightly greater than the elastic thickness, but about one-half the seismic (surface wave) thickness.

Lithospheric deformation is thought to be controlled by the variation with depth of strength (the maximum difference between principal stresses that rock can support). The earthquake depth data suggest that above about 750°C the lithosphere cannot support stresses needed for seismic failure. Experimental data (Brace and Kohlstedt, 1980; Kirby, 1980) can be used with a geotherm to compute strength as a function of depth (Fig. 5): at shallow depths brittle fracture occurs and strength increases linearly with depth. At greater depths strength is controlled by ductile flow laws, which vary with mineral type; since strength decreases exponentially with temperature, rocks weaken rapidly with depth. Thus, as the plate ages and cools, the strong portion of the lithosphere deepens (Fig. 5).

In the ductile domain, strength depends on strain rate: thus flexural thickness from long-term loads (at low strain rates) is less than the thickness measured with surface waves, corresponding to shorter-term loads or high strain rates. This explains why the responses of the plate to loading by a new volcanic island (which may take typically 1 Ma to grow) and to the passage of a surface wave (of typical period 100 s) differ drastically. The strain rates for intraplate deformation shown on Fig. 5 were estimated from the rate of seismic moment release of oceanic intraplate earthquakes: the lower value, $10^{-18}\,s^{-1}$, is for the oceanic lithosphere as a whole; the upper value, $10^{-15}\,s^{-1}$, is for a very active zone of intraplate deformation, the Ninetyeast Ridge area (Stein and Okal, 1978).

The relationship between results derived in the laboratory (and extrapolated to geological strain rates) and the actual behavior of materials in the Earth is somewhat unclear. Nonetheless, it is useful to be able to relate the depth of seismicity to strength envelopes that can be calculated for different thermal and mechanical situations and compared between tectonic environments.

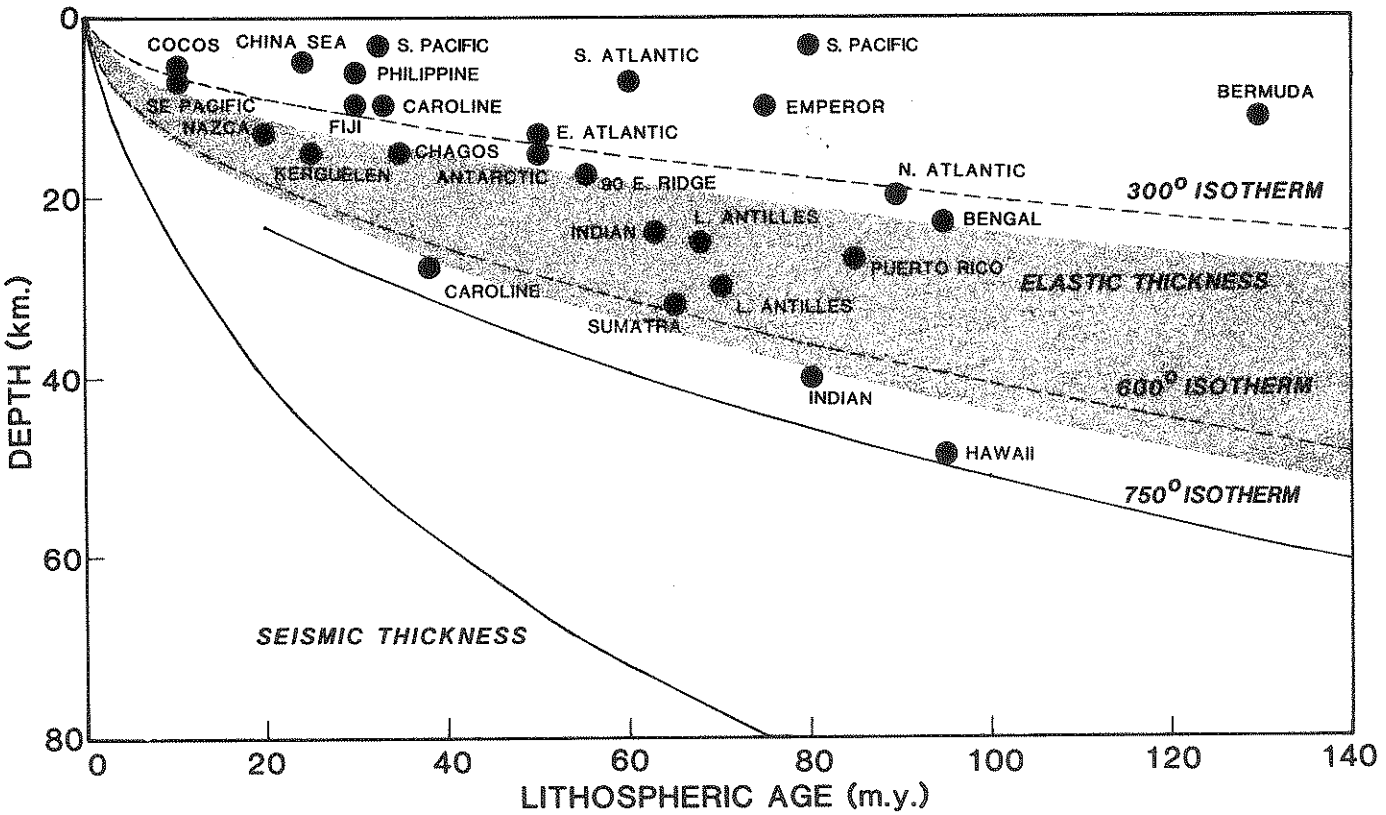

Fig. 4. The maximum depth of intraplate earthquakes deepens as the oceanic lithosphere cools (Wiens and Stein, 1983). The isotherms shown are calculated from a lithospheric cooling model (Parsons and Sclater, 1977). Stippled region denotes range of estimates of the flexural elastic thickness. The seismic thickness is taken from Rayleigh wave dispersion data. The failure limit is the lower limit at which 20 MPa (200 bar) deviatoric stress can be sustained for a dry olivine rheology and a strain rate of 10^{-18} s^{-1}.

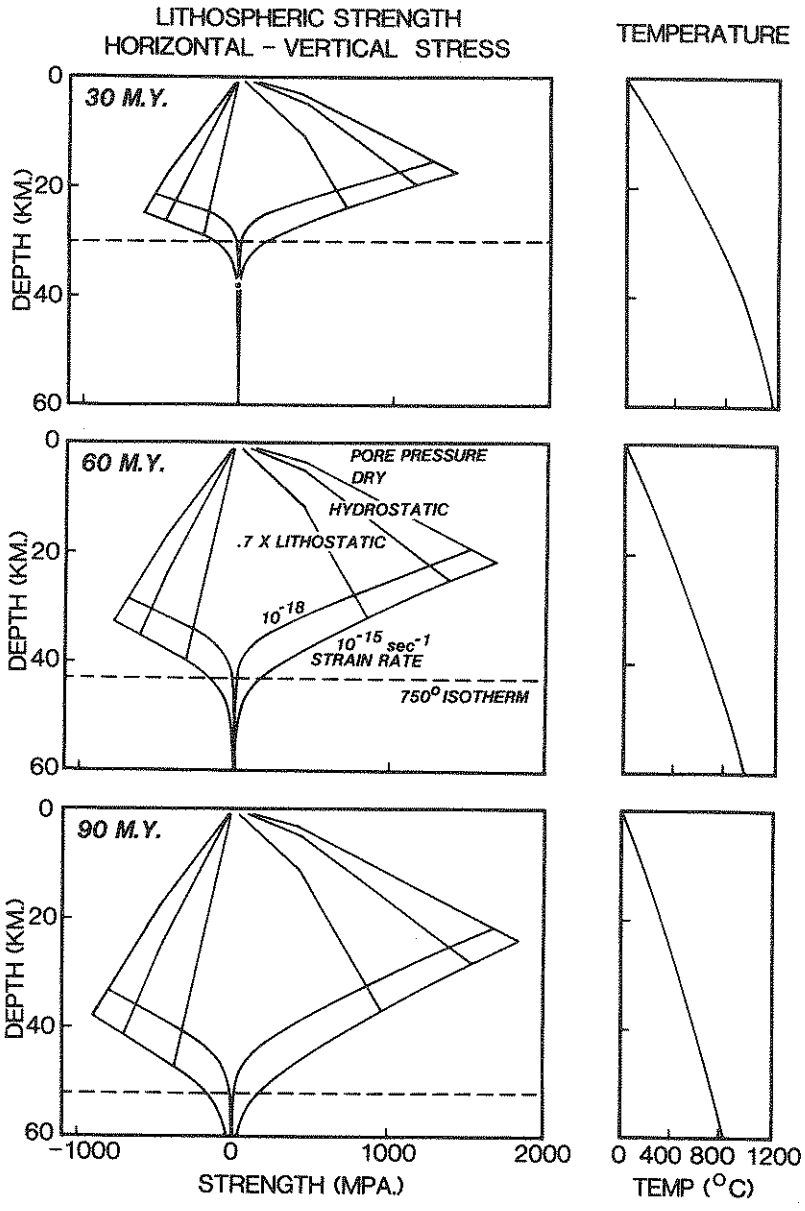

Fig. 5. Strength envelopes showing maximum stress difference as a function of depth calculated using temperatures from the Parsons and Sclater (1977) plate cooling model (Wiens and Stein, 1983). At shallow depth strength is controlled by brittle fracture; at greater depth ductile flow laws predict rapid weakening. The 750°C isotherm (dashed line) is the approximate lower bound for intraplate seismicity. The strong region deepens as the plate cools.

B. Focal Mechanisms and Intraplate Stresses

Stresses inferred from mechanisms of oceanic intraplate earthquakes can be used to study the forces acting on the plates. A major difficulty in inferring stresses from mechanisms is the concentration, discussed later, of seismicity on pre-existing weak zones and its relation to local tectonics. Nonetheless, a natural approach is to use the full data set while avoiding reliance on individual mechanisms.

Since the forces acting on the lithosphere are controlled by its thermal evolution, it is natural to study intraplate seismicity as a function of lithospheric age. The level of intraplate seismicity decreases with age (Fig. 6). The seismicity rate seems relatively constant between 40 and 90 Ma, but is much higher for young lithosphere and much lower for old lithosphere. The rate per unit volume above the 750°C isotherm also decreases. The exclusion from studies of intraplate seismicity of events closer than 100 km to the ridges shows that the high seismicity rate in young lithosphere (5–15 Ma) is genuine, and does not result from mislocated ridge events.

Figure 7 shows the variation of mechanism type with lithospheric age (Wiens and Stein, 1985). Lithosphere older than about 35 Ma is in horizontal deviatoric compression, as shown by thrust and strike-slip mechanisms. Mendiguren (1971) and Forsyth (1973) noted compression in approximately the spreading direction, and related it to the "ridge push" gravitational force due to lithospheric cooling and subsidence (Lister, 1975; Parsons and Richter, 1980).

Seismicity in younger lithosphere is more complex and not fully understood. Sykes and Sbar (1974) suggested a transition at about 20 Ma from spreading-related extension to compression. Recent analyses show a more complex picture (Wiens and Stein, 1984; Bergman and Solomon, 1984). Both compression and extension are observed in young lithosphere, with most extensional events occurring in the central Indian Ocean. In young lithosphere elsewhere, faulting is often concentrated in small seismically active regions, where mechanisms can be extremely heterogeneous.

The high seismicity in young lithosphere suggests that near-ridge stress sources, rather than plate-wide processes, produce much of this seismicity. These effects may include thermoelastic stress (Turcotte and Oxburgh, 1973; Bratt *et al.*, 1985) and stresses associated with ridge-transform intersections (Fujita and Sleep, 1978). However, some information about plate-wide stresses can be extracted from earthquakes in young lithosphere. In lithosphere younger than 35 Ma, tensional axes of normal fault events are oriented at large angles to the spreading direction (Fig. 8); these earthquakes thus *cannot* indicate ridge-related extension. In addition, no age boundary

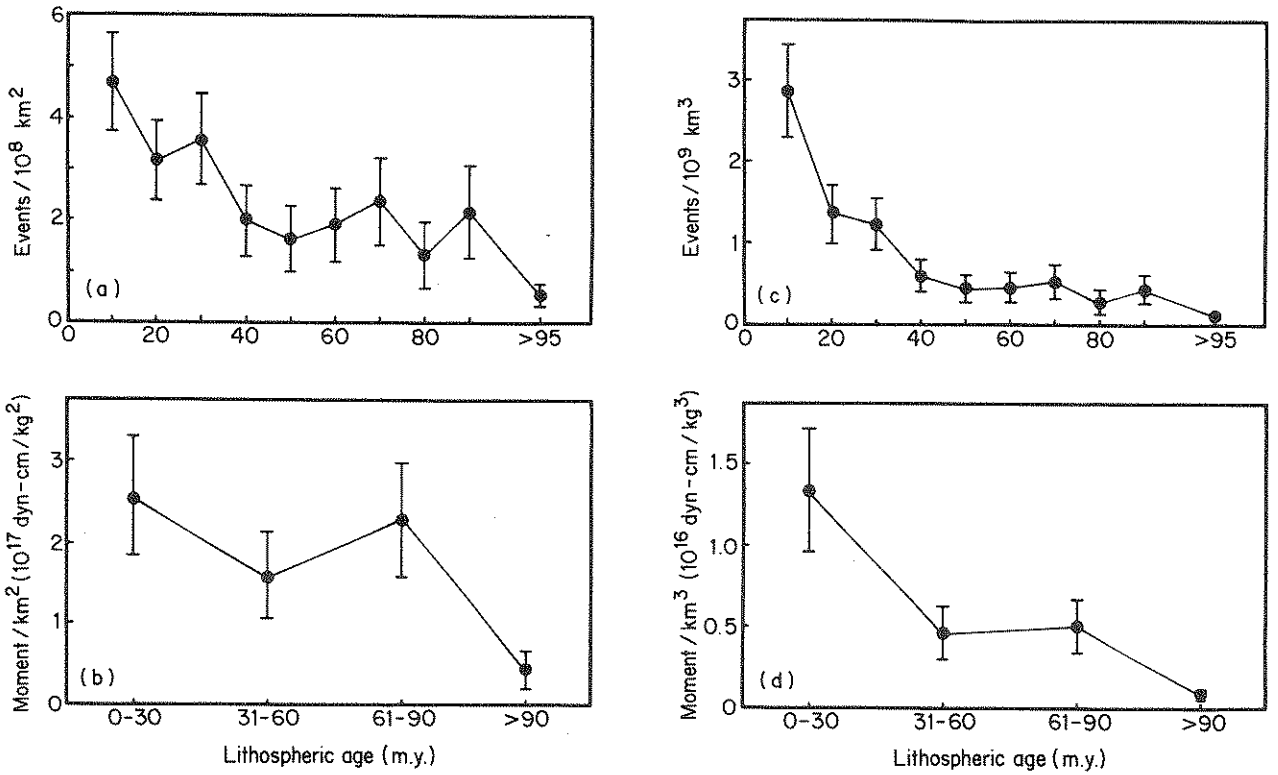

Fig. 6. Decrease in oceanic intraplate seismicity with lithospheric age for the period 1964–1979 (Wiens and Stein, 1983). (a) Number of oceanic intraplate earthquakes with m_b above 5.0 per surface area versus age. (b) Number of intraplate earthquakes per volume of strong lithosphere (that above the 750° isotherm) versus age. Cumulative seismic moment of oceanic intraplate seismicity per area (c) and volume (d) as a function of age.

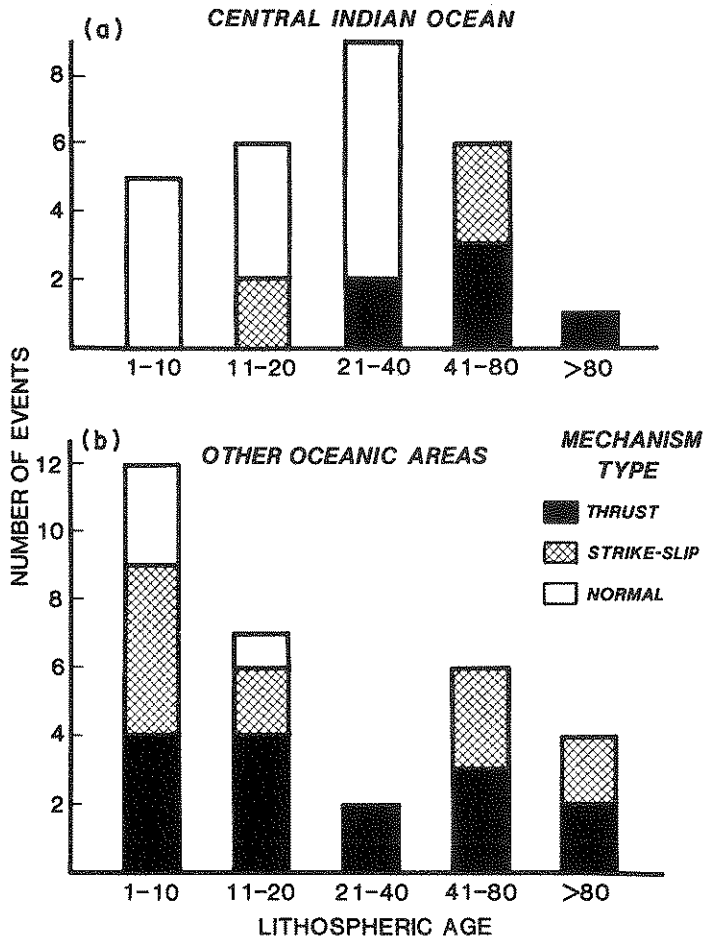

Fig. 7. Focal mechanism type as a function of lithospheric age for oceanic intraplate earthquakes (Wiens and Stein, 1984). Older oceanic lithosphere is in compression, whereas younger lithosphere has both extensional and compressional mechanisms. Extensional events are located primarily in the Central Indian Ocean.

between compressional and tensional earthquakes can be drawn, as both types can coexist in any area younger than about 35 Ma. A two-dimensional "average" plate can therefore be modeled with a general compressional stress in the spreading direction for all ages. Such models do not include the tensional stress parallel to the ridge in young ($\leq$35 Ma) areas.

Assuming that the plate is in equilibrium, a simple two-dimensional model shows that stress is determined by the ridge-push force and by boundary

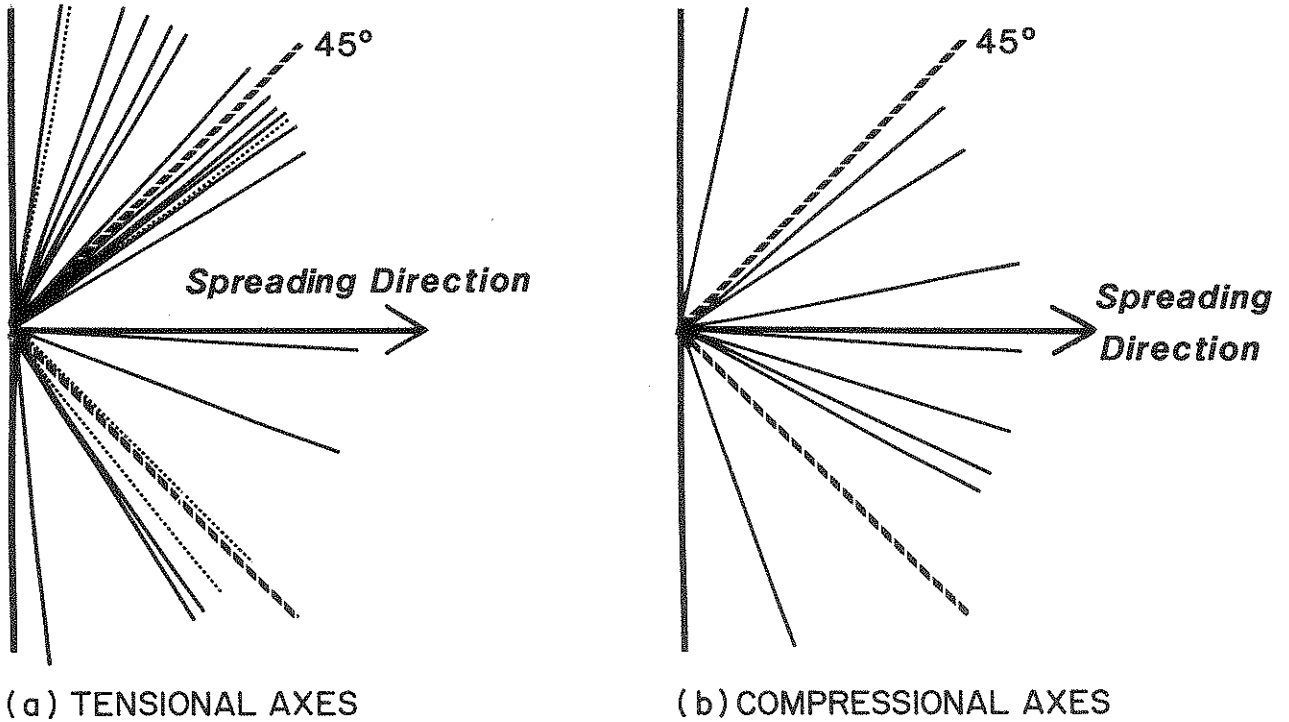

Fig. 8. Angle between the horizontal component of principal stress and the spreading direction for normal faulting (a) and thrust faulting (b) intraplate earthquakes in young oceanic lithosphere (Wiens and Stein, 1984). Tensional axes of normal faulting events, most of which are located in the Central Indian Ocean, generally show extension oblique to the spreading direction, while compressional axes of thrust faulting events show a weak preferred orientation in the spreading direction [Central Indian Ocean (——); Other regions (· · · · ·)].

conditions at the ridges and bottom of the plate (Mendiguren and Richter, 1978; Wiens and Stein, 1985). The deviatoric compression observed for all ages in the direction of spreading (x) can be compared to the predicted deviatoric stress $\overline{\sigma_{xx}}$ averaged over the lithospheric thickness $h(t)$ at age t. This stress shows the balance between the ridge-push force $F(t)$ and the drag at the base of the plate. For an absolute velocity v (taken as the half spreading rate), the basal drag (assumed constant) equals the product of velocity and drag coefficient C, so that:

$$\overline{\sigma_{xx}}(t) = \frac{Cv^2t - F(t)}{h(t)}$$

Both the lithospheric thickness (defined as depth to an isotherm) and the ridge-push force depend on thermal structure. For a cooling half-space model (Turcotte and Oxburgh, 1967), lithospheric thickness increases as the square root of plate age $\sqrt{t}$ and the ridge-push force increases linearly with age t (Lister, 1975). Figure 9 shows intraplate stress as a function of age and drag coefficient. For zero drag the stress from ridge-push alone is purely compressive ($\overline{\sigma_{xx}} < 0$) and varies as $\sqrt{t}$, since force increases linearly while thickness increases as the square root. If the drag coefficient C is increased, $\overline{\sigma_{xx}}$ follows $\sqrt{t}$ curves corresponding to less and less compression, until the lithosphere is in extension for all ages. All lithospheric plates are known to be in compression, and thus a rapidly moving plate (e.g. Pacific, 10 cm/yr) constrains the drag coefficient C to less than about 3.5 MPa/(m/yr), and basal stress to less than 0.35 MPa (3.5 bar). In contrast, a plate moving 10 times slower can remain in compression with a drag coefficient 100 times greater and a basal stress 10 times greater.

For a cooling plate model, both the lithosphere thickness and ridge-push force approach asymptotic values with age (McKenzie, 1967; Parsons and Richter, 1980). As a result, stress need not be monotonic with age. For no drag ($C = 0$), stress becomes more compressive with age, but for larger drag, stress reaches a compressional maximum, becomes less compressive, and eventually extensional. The maximum drag coefficient allowing compression is about half that for half-space models. Assuming the same drag coefficient for all plates yields a maximum drag coefficient of about 2–4 MPa/(m/yr); the ridge-push force dominates drag for all ages. If the drag coefficient is constant for all plates, basal drag is much less significant for slow plates than for fast ones.

This model assumes a zero stress boundary condition at the ridge, or in other words, that the ridge axis has no tensile strength. However, stress in a young lithosphere, especially the location of a possible transition from compression to extension in the direction of spreading, would be sensitive

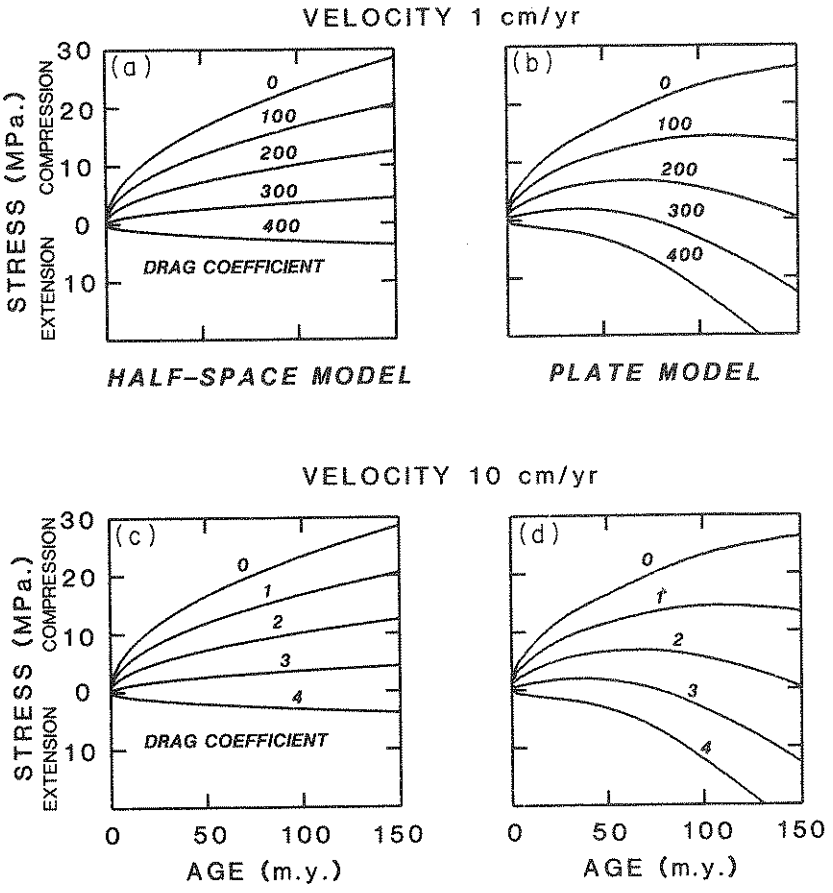

Fig. 9. Intraplate stress as a function of lithospheric age and assumed basal drag coefficient for slow moving (a, b) and fast moving (c, d) plates (Wiens and Stein, 1985). Figures (a) and (c) assume a half-space thermal model; Figures (b) and (d) assume a plate model. The observation of compressional stresses in oceanic lithosphere places an upper bound on the drag coefficient of 2–4 MPa/(m/yr).

to the strength of the ridge (Fig. 10). Alternative models with a tensile stress boundary condition, i.e. substantial strength in the axial region (Fleitout and Froidevaux, 1983), would predict a wide band of intraplate extension in the spreading direction. Since such a zone of normal faulting is not observed, the axial region must have little tensile strength, a useful constraint on ridge models (Sleep and Rosendahl, 1979). Figure 11 summarizes the different tectonic constraints.

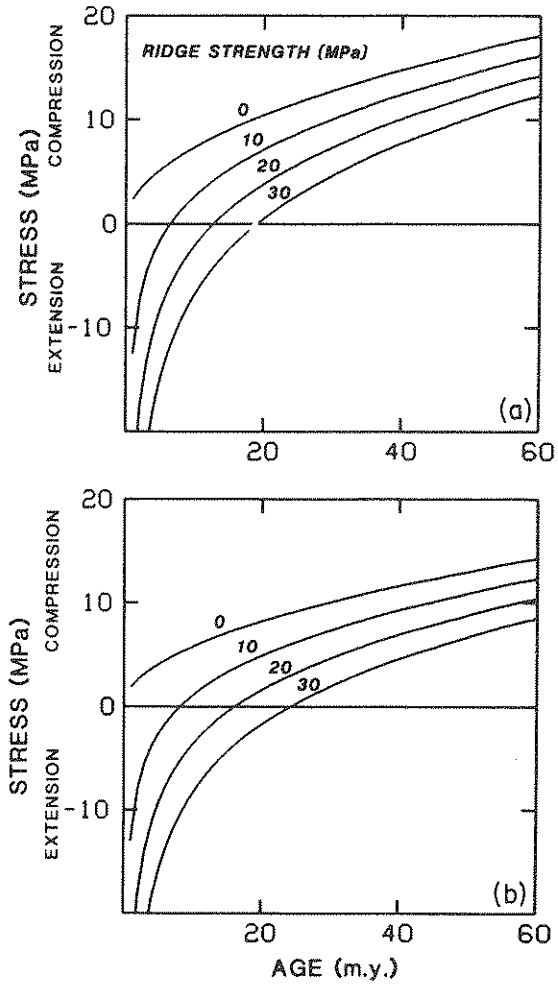

Fig. 10. Vertically averaged stress in the spreading direction as a function of lithospheric age computed for a plate velocity of 5 cm/yr and several values of ridge strength and basal drag (Wiens and Stein, 1985). The age of the transition from ridge-normal extension to compression increases with the strength of the ridge [(a) No basal drag and (b) drag coefficients 3 MPa/(m/yr)].

C. Constraints on Mantle Viscosity

Earthquake mechanisms, though not a primary tool for estimation of mantle viscosity, provide interesting inferences under certain assumptions. The analysis assumes a common model of plate motions driven largely by thermal buoyancy forces acting on the lithosphere with mantle return flow balancing

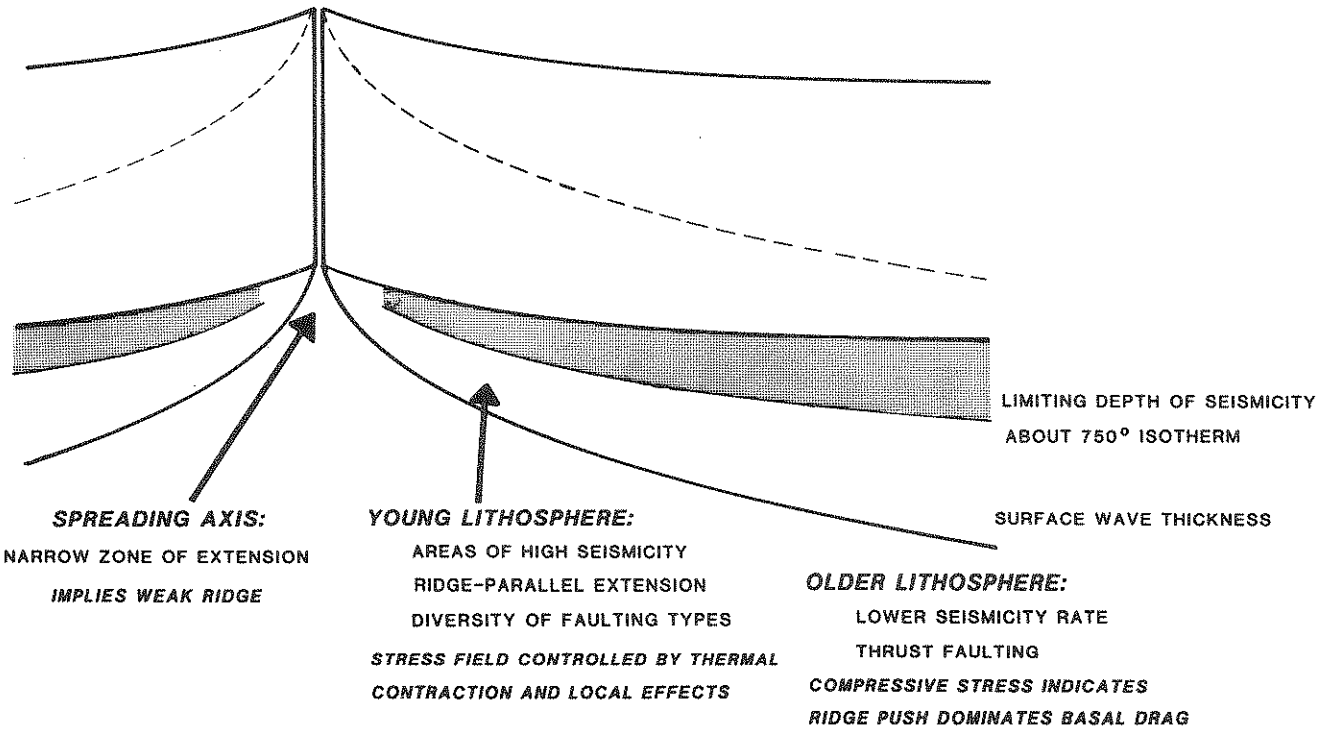

Fig. 11. Schematic diagram relating seismicity observations to the tectonics of the oceanic lithosphere (Wiens and Stein, 1985).

the mass transport due to plate motions. [An alternative model (Peltier, 1980) assumes that convective mantle flow provides an active mechanism for driving plate motions.] If the drag on the base of a plate is due to motion over the viscous mantle, compressive earthquake mechanisms in old lithosphere constrain the viscosity structure (Mendiguren and Richter, 1978; Wiens and Stein, 1985). It is useful to consider a simple two-dimensional geometry where mass flux due to the moving plate is balanced by a return

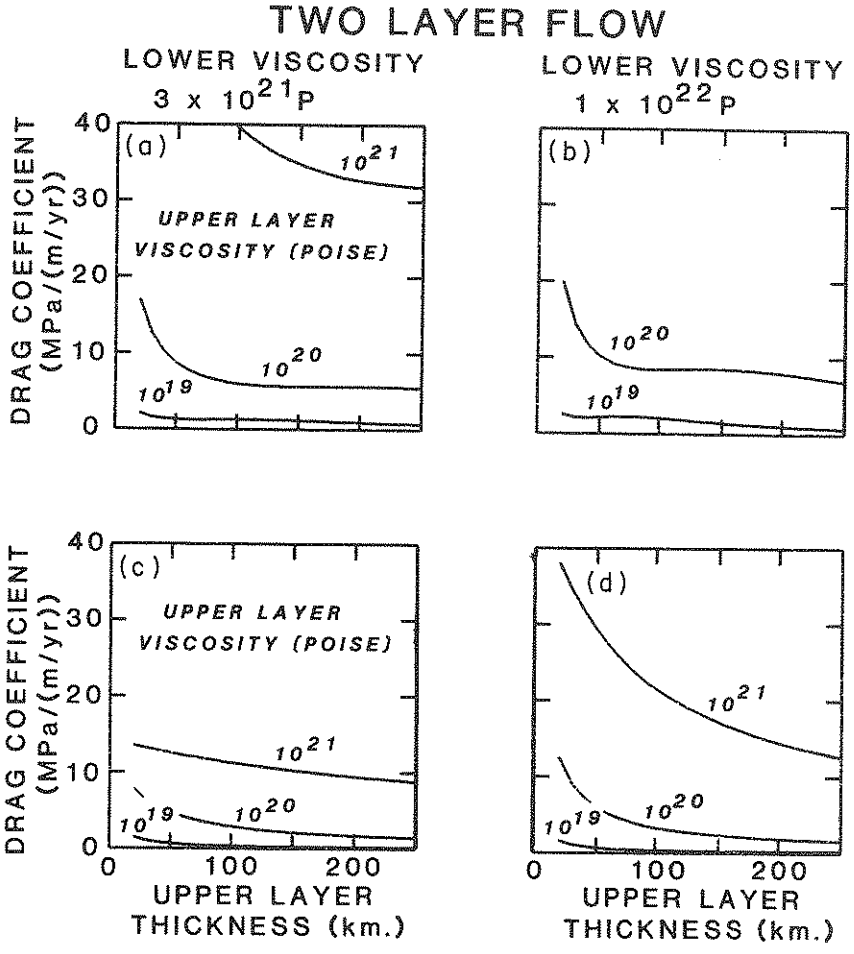

Fig. 12. Basal drag coefficients as a function of upper layer (asthenosphere) thickness and viscosity for two values of lower layer viscosity and total flow depths of 700 km (a, b) and 2900 km (c, d). The upper bounds on drag coefficients required by the focal mechanism data constrain the mantle viscosity. (Wiens and Stein, 1985).

flow at depth. The drag coefficient is proportional to viscosity and inversely proportional to flow depth. For the simplest case, in which the underlying fluid has uniform Newtonian viscosity, acceptable drag values require an average mantle viscosity significantly lower than estimated from glacial rebound, Earth rotation and satellite orbits.

This discrepancy can be reconciled by assuming that the plate is underlain by a thin low-viscosity asthenosphere. Such a model satisfies constraints from gravity (Richter and McKenzie, 1978), driving forces (Hager and O'Connell, 1979) and glacial isostasy (Cathles, 1975; Peltier, 1983). In this model the low-viscosity layer, in which only a fraction of the return flow occurs, decouples the plates from the underlying mantle. For a mantle (lower layer) with viscosity 3×10^{21} P, acceptable drag coefficient values occur for asthenospheric (upper layer) viscosities less than about 6×10^{19} P for upper mantle return flow and 2×10^{20} P for the whole mantle case (Fig. 12). For a more viscous mantle, the maximum acceptable asthenospheric viscosities decrease. The low-viscosity layer significantly reduces the effect of the total flow depth so that either upper mantle or whole mantle flow is acceptable. These viscosity bounds are for oceanic regions and may not be comparable to those for continental regions.

These simple calculations provide only general estimates of viscosity structure. In particular, the assumed two-dimensional flow is reasonable for large plates overlying a low-viscosity asthenosphere but less valid for smaller plates or a higher-viscosity atmosphere (Hager and O'Connell, 1979). Even if the drag coefficient is spatially uniform, the apparent drag would vary when the return flow is not antiparallel to the plate's absolute motion. Additionally, the temperature dependence of viscosity should lead to structures more complicated than simple layers. Nonetheless, intraplate stresses derived from earthquake focal mechanisms can be explained by conventional ideas of mantle viscosity and support a low-viscosity layer below the oceanic plates. Such decoupling is consistent with the lack of correlation between oceanic plate area and absolute velocity (Forsyth and Uyeda, 1975).

IV. Plate Boundary Processes

A. Ridge–Transform Systems

Earthquake seismology has also considerably improved our knowledge of oceanic spreading center systems. Early studies (Sykes, 1967) identified normal faulting on some mid-ocean ridges; such earthquakes are now known to be confined to slow-spreading ridges (less than about 6 cm/yr full rate), also characterized by axial valleys. Figure 13 shows a decrease in seismic

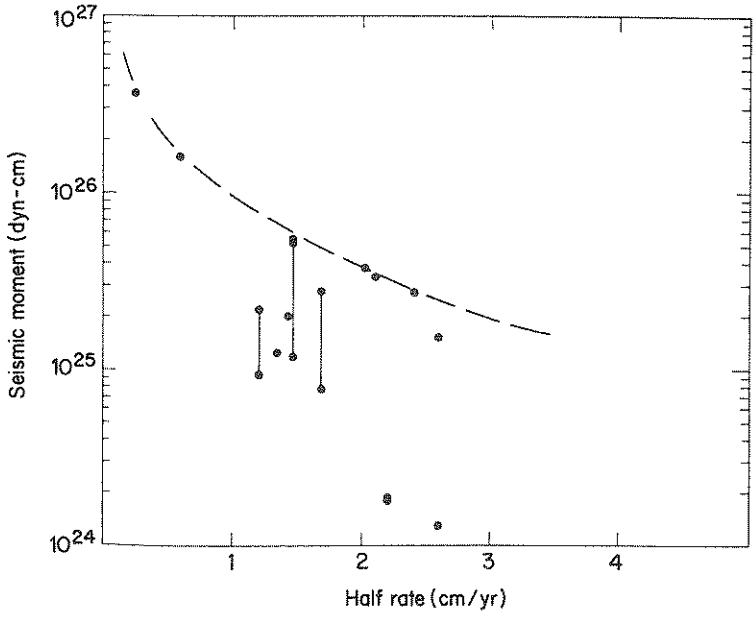

Fig. 13. Decrease in maximum seismic moment of ridge-crest normal fault earthquakes with spreading rate (Solomon and Burr, 1979).

moment of ridge-crest normal faulting earthquakes with spreading rate. This relation is consistent with faulting which is limited by temperature; the depth to a given isotherm and hence the area available for faulting decreases with spreading rate (Solomon and Burr, 1979). Fast-spreading ridges show an axial high, rather than a valley, and thus no normal faulting events.

Despite the presence of topography suggestive of vertical tectonism at transforms [notably anomalously high features (Bonatti, 1978)], detailed focal mechanism studies (Fig. 14) show almost no deviations from the transform-parallel strike–slip motion on steeply dipping fault planes predicted by Wilson (1965). The only exceptions occur at ridge–transform intersections (Fig. 15), which show a variety of tectonic anomalies due to the cooling of the ridge as it approaches an intersection (Fox and Gallo, 1984; Forsyth and Wilson, 1984).

The thermal structure of a transform fault should be essentially the average of the expected temperature on the two sides; coolest at the transform midpoint and hottest at either end (Fig. 16). As expected from the area available for faulting, the maximum seismic moment for transform earthquakes decreases with spreading rate (Fig. 17) (Burr and Solomon,

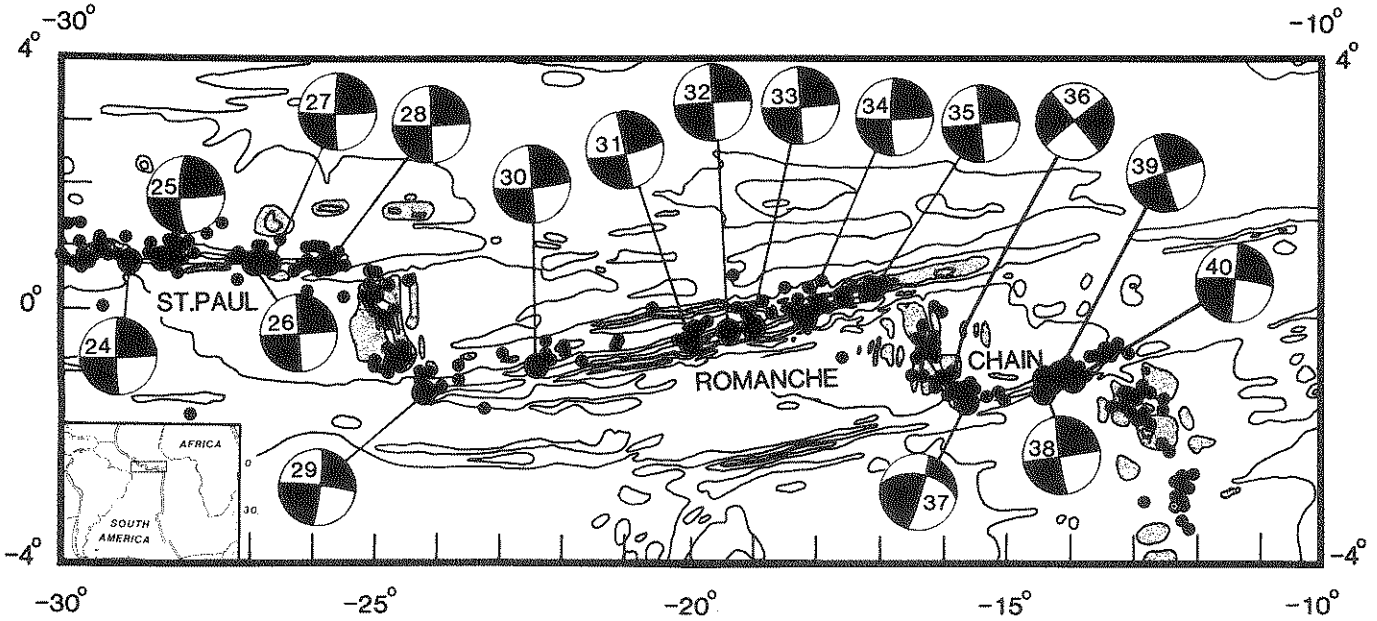

Fig. 14. Earthquake focal mechanisms on equatorial Atlantic transform faults (Engeln *et al.*, 1986). The vast majority of events show the expected transform–parallel strike–slip faulting on a steeply dipping plane. Note anomalous mechanism events near the west end of the Chain transform

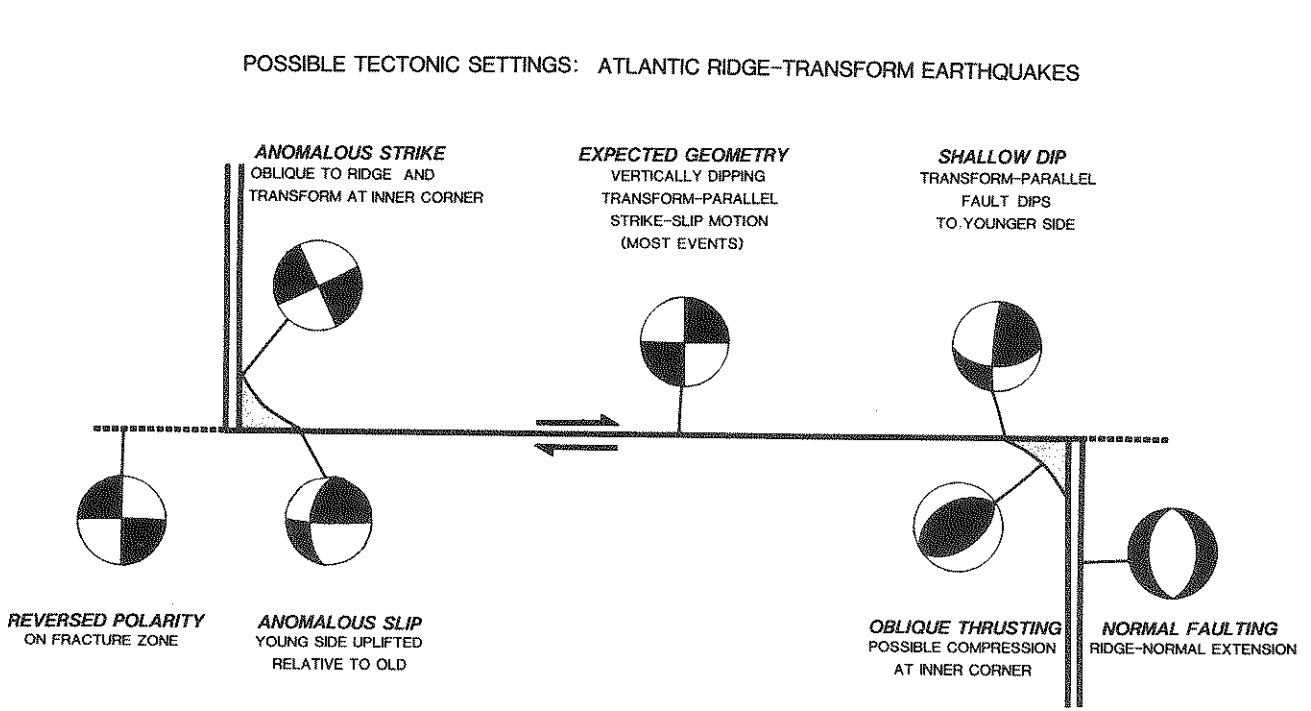

Fig. 15. Schematic transform showing possible tectonic settings of Atlantic ridge–transform earthquakes (Engeln *et al.*, 1986). Most transform events show the expected geometry. Anomalous geometry events occur only near the ridge–transform intersections and may be related to faulting at the inner corner.

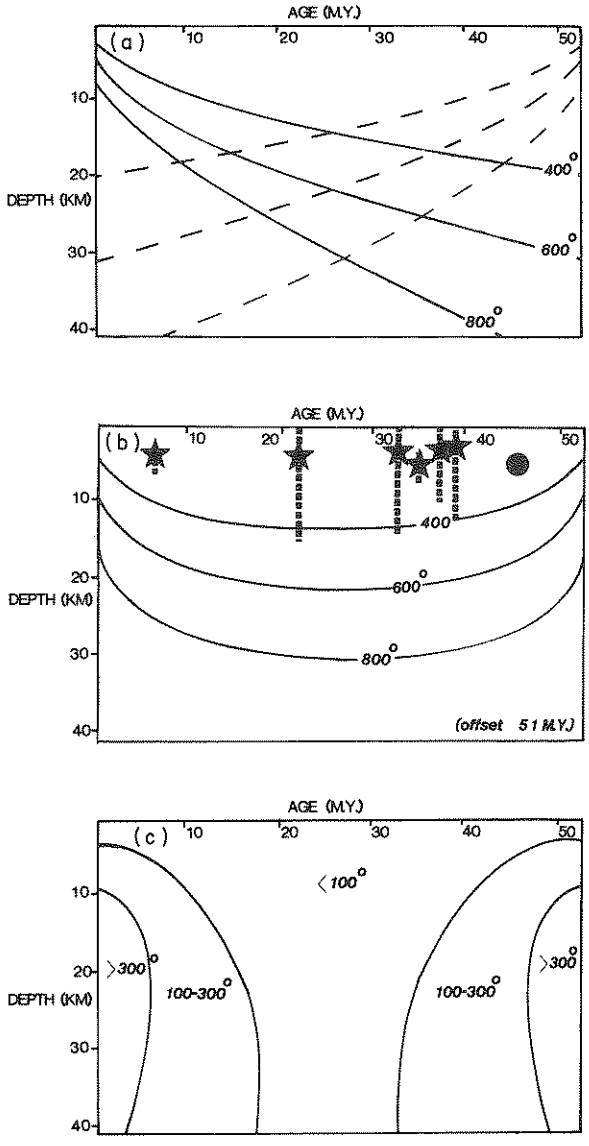

Fig. 16. Thermal structure of the Romanche Transform. (a) Temperatures on either flank predicted by the cooling half-space model. (b) Average temperature distribution along the transform. Stars represent the locations and depths of the well-constrained earthquakes; dots represent events with less reliable depths. Dashes represent the depth range of faulting estimated from the seismic moments. All centroid depths are above the 400° isotherm predicted by the thermal model and most faulting is above the 600°C isotherm. (c) Difference between transform and cooling half-space temperatures (Engeln *et al.*, 1986).

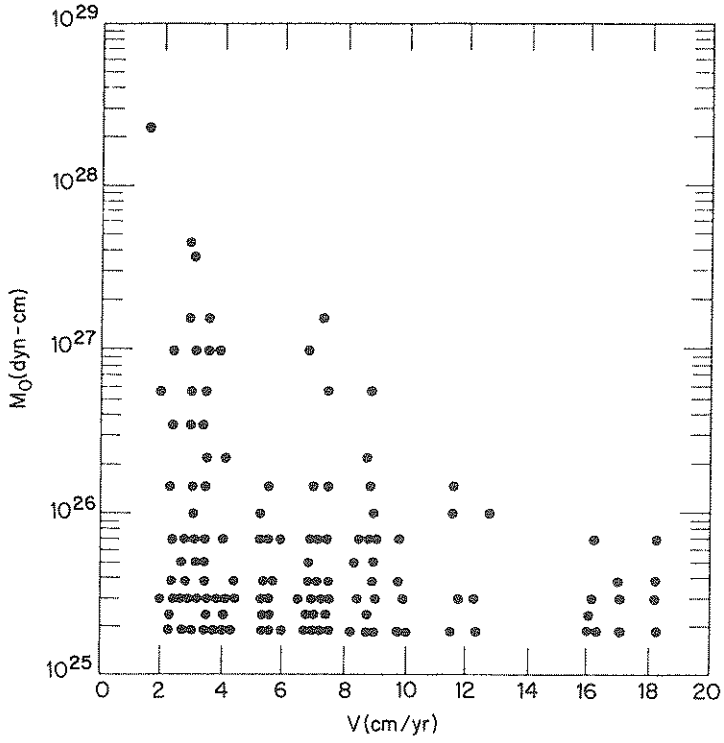

Fig. 17. Seismic moment versus spreading rate for oceanic transforms (Solomon and Burr, 1979). The maximum moment decreases with spreading rate as expected from thermal considerations.

1978). Centroid depths of transform earthquakes (Figs. 16 and 18) are limited to a shallow zone above the predicted 400°C isotherm. The depth range of faulting estimated from the seismic moments suggests that faulting extends approximately down to the 600°C isotherm.

The depth of seismicity has interesting implications for the slip process on transforms. Given the depth of faulting, slip rates can be inferred from seismic moment release and compared to those predicted by plate motions. Assuming that the areas above either the 400°C or 600°C isotherms fail seismically, seismic moment releases for six major Atlantic transforms covering the period 1920–1979 account for varying fractions of the slip predicted by the plate motion (Fig. 19). Some aseismic slip must be occurring if the time period sampled is long enough to be representative. An earlier analysis, predating precise constraints on depths of transform earthquakes, which assumed that all slip was seismic, implied faulting to an average depth approximately that of the 150°C isotherm (Burr and Solomon, 1978). In

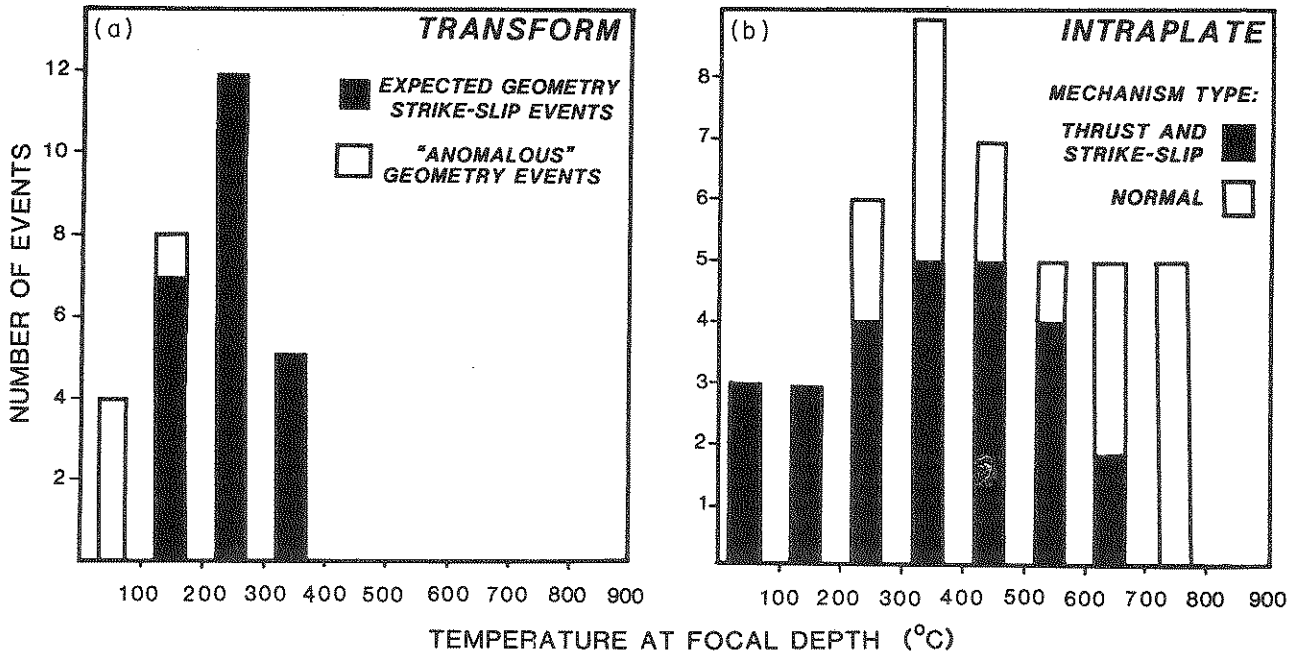

Fig. 18. Comparison of transform (a) and intraplate (b) earthquake depths (Engeln *et al.*, 1986). Centroid depths along transforms are confined to a zone above the 400°C isotherm (a) and concentrated between 100° and 300°C. In contrast, oceanic intraplate seismicity (b) occurs primarily between the 300°C and 600°C isotherms and is limited by the 750°C isotherm (Wiens and Stein, 1983, 1984).

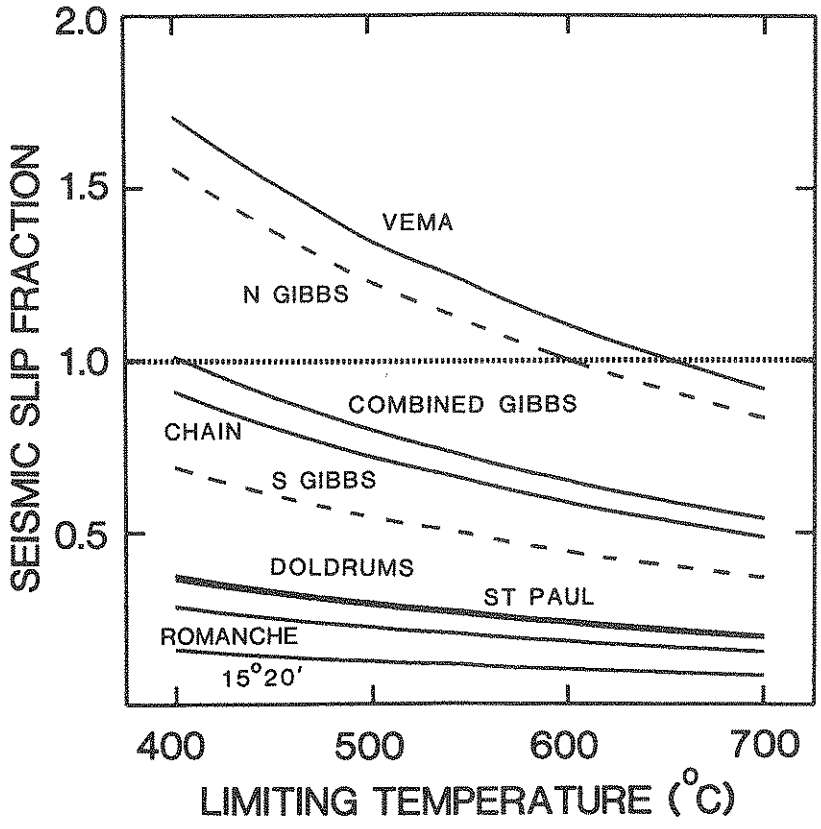

Fig. 19. Fraction of seismic slip (seismic slip rate divided by predicted plate motion) versus limiting isotherm for major Atlantic transforms. Five of the seven have significant aseismic slip if the 400°C isotherm is used. If the 600°C isotherm suggested by the lower limit of faulting (Figs. 16 and 18) is used, all transforms except the Vema have some proportion of aseismic slip. The Vema may have a larger than estimated fault area due to tectonic complications. Because a short offset in the Gibbs Transform makes it unclear whether it should be regarded as one or two transforms, results are shown for both cases (Engeln *et al.*, 1986).

the absence of focal depth interpretation, these are two essentially equivalent ways of viewing the same data, since there is a complete trade-off between the assumed "average" depth of slip and the fraction of slip taken up seismically.

It is unclear what causes the variation in the seismic fraction of slip or equivalently in depth extent of slip. The Vema Transform is a clear example; inferred seismic slip is substantially greater than predicted unless faulting extends to the 650°C isotherm. Transforms may differ substantially; the

Vema may have an unusually long recurrence time or be mechanically anomalous due to its complex tectonic history.

Full understanding of the transform slip process requires knowledge of thermal and mechanical structure. If centroid depths reflect strength as a function of depth, these can offer some insight (Fig. 18). In contrast to transform events, centroid depths for oceanic intraplate earthquakes extend down to approximately the 750°C isotherm. Transforms have much higher strain rates ($10^{-13}\,s^{-1}$) than intraplate areas ($10^{-18}\,s^{-1}$), so if both were characterized by the same dry olivine rheology, the limiting isotherm for transforms should be higher, approximately 1000°C. Alternatively, if a weaker hydrated olivine rheology was more appropriate for transforms, the higher strain rate should cancel the weakening effect and yield a limiting isotherm similar to that for intraplate regions.

Thus, transforms may either have much higher temperatures than expected and/or be much weaker than expected. In the former case, the required anomalously high temperatures, perhaps due to intrusion at depth below transforms, predict measurable heat flow anomalies. The second possibility, unusual rheological weakness, is reminiscent of the unexplained weakness of the San Andreas transform, where heat flow data exclude anomalously high temperatures (Lachenbruch and Sass, 1980). Several lines of inquiry such as teleseismic earthquake studies, ocean bottom seismometer surveys and adequate heat flow should help advance our understanding of the thermal structure and mechanical process on oceanic transforms.

B. Evolution of Ridge–Transform Systems

Seismological studies of rapidly changing ridge-transform systems offer some insights into the process by which plate boundaries evolve. For example, along the East Pacific Rise (EPR) near the location of the fastest spreading currently observed, bathymetric, seismic and magnetic data suggest the existence of two small plates between the Nazca and Pacific Plates (Herron, 1972; Forsyth, 1972). Anderson *et al.* (1974) suggested that the southern boundaries of the northern microplate, known as the Easter Plate, were stable spreading centers joined to the EPR on the north by long transforms. In contrast Handschumacher *et al.* (1981) interpreted the eastern boundary as a propagating rift (Hey, 1977), growing northward at the expense of the west ridge.

The concentration of seismicity along the boundaries suggests a rigid platelet, rather than a diffuse deformation zone. Focal mechanism data can be combined with marine geophysical results to suggest the nature of its boundaries. The east ridge spreading rapidly shows the low seismicity

expected for a fast ridge. The southwest boundary is the most active seismically; its normal faulting events suggest slow spreading, by analogy to the Mid-Atlantic Ridge, whereas the strike-slip events suggest transform motion. The northeast boundary, on which both thrust and strike-slip motions occur, is unclear and may be a more diffuse deformation zone.

Treating the Easter Plate as rigid, relative motions between the Easter, Nazca and Pacific Plates can be determined by inversion, using Minster and Jordan's (1978) algorithm (Fig. 20). The proximity of the Easter–Nazca and Easter–Pacific poles allow significant variation in relative motion along the boundaries. The model predictions are generally good; spreading rates decrease rapidly to the north along the East ridge. The Easter–Pacific pole fits the observed rate on the northwest boundary and predicts slow spreading on the southwest boundary. The transform direction implied by the strike-slip events on the southwest boundary is fit well and spreading is predicted to be slightly oblique. The northwest boundary (or diffuse boundary zone) remains unclear, with the predicted motions changing from oblique convergence to strike-slip to oblique divergence. Recent detailed magnetic and bathymetric surveys (Naar and Hey, 1986) of the east ridge should provide the basis for a more accurate model.

The Easter Plate situation may be a model for the evolution of an area where one spreading center is being born and another dies. Figure 21 illustrates the schematic evolution of such a plate for a simple geometry similar to the Easter Plate. As a new spreading center develops, the old one adjusts to keep the total spreading rate and direction constant between the two large plates. Since the propagating rift spreads orthogonally, the dying ridge slows and changes spreading direction. Relative motion across the original transform also changes during propagation. Since motion across the original transform is no longer parallel to this boundary, the transform evolves into a "leaky" transform (Menard and Atwater, 1968) and then to a ridge spreading nearly orthogonally.

Comparison of this model with the Easter and Galapagos situations suggests that the dominant factor determining the ultimate fate of the platelet is its size. The more lithosphere is present, the more difficult it is for this area to be sheared. Thus, while small-scale ridge overlaps appear to have extensively sheared regions between ridges (Macdonald and Fox, 1983), large-scale propagation will tend to produce rigid plates. Microplates have been identified in magnetic anomalies when major boundary reorganizations shifted material from one large plate to another (Menard, 1978; Mammerickx *et al.*, 1980; Cande *et al.*, 1982). If the Easter analogy is valid, such microplates may be the mechanism by which large-scale ridge boundary reorganizations occur.

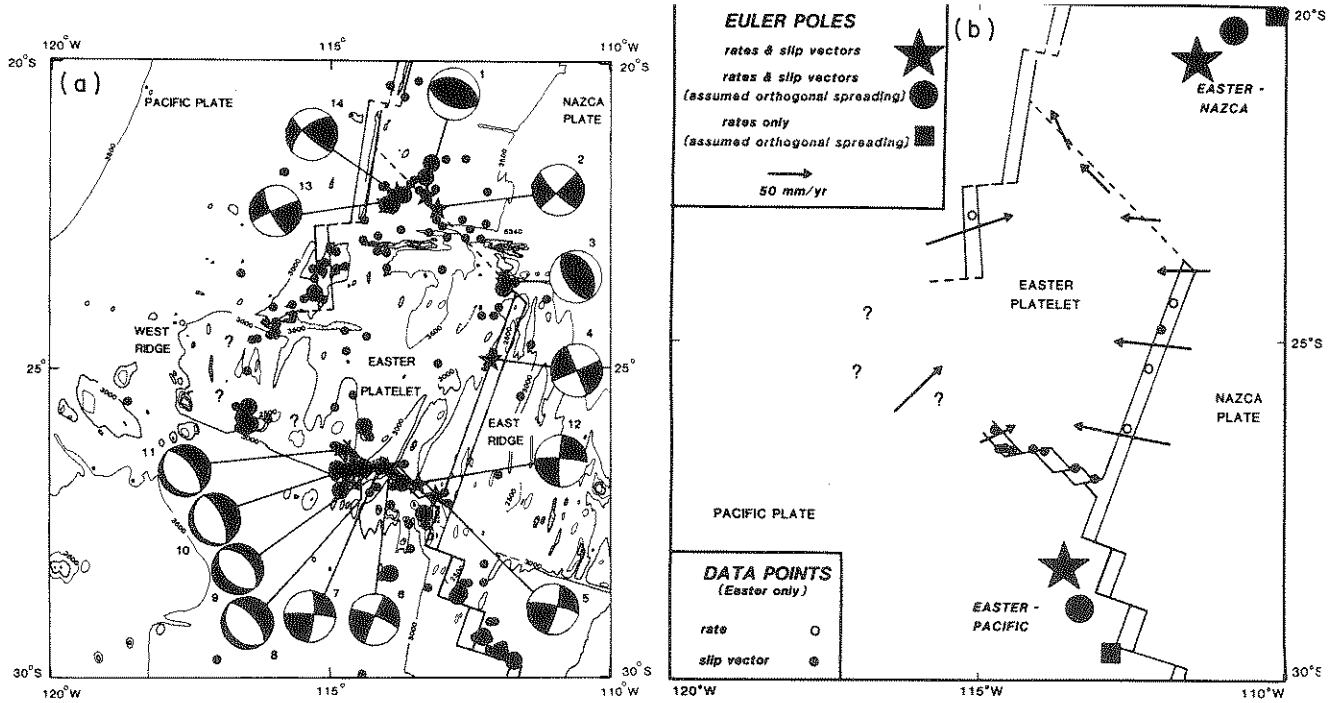

Fig. 20. (a) Bathymetry, seismicity and tectonics of the Easter Plate. Dots represent earthquake epicenters for the period 1963–1978; larger dots indicate events with $m_b > 5.1$. The stars represent earthquakes whose mechanisms have been determined. The East Ridge, the northern West Ridge and the southwest boundary are constrained by geophysical or seismological data; the other boundaries are less well known. (b) Rigid plate analysis of the Easter Plate system showing the Euler poles for different subsets of the data. The motions of the Easter Plate relative to the Nazca and Pacific Plates predicted using all of the data are indicated by the arrows. The open and closed circles represent the locations of rate or slip vector measurements (Engeln and Stein, 1984).

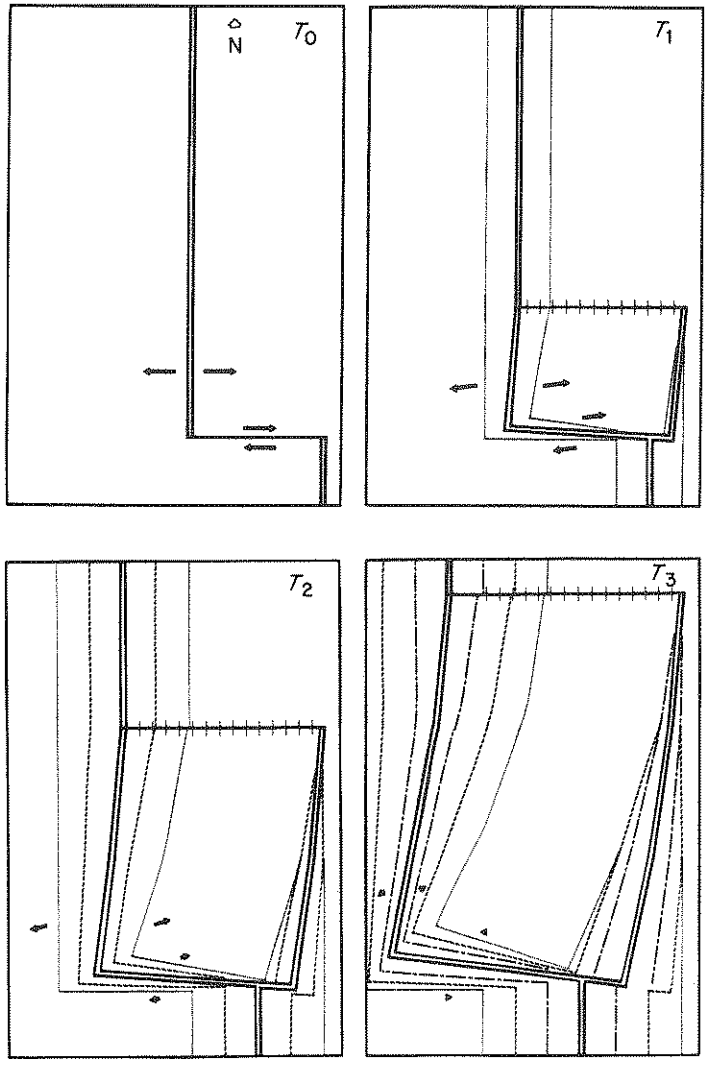

Fig. 21. Schematic evolution of a rigid microplate at a spreading center. The propagating rift spreads orthogonally and reaches full spreading at its base at time T3. Spreading on the dying ridge becomes more oblique (arrows) while the transform changes into a ridge which approaches orthogonal spreading over time. The difference in spreading rate at the base of the propagator offsets the propagating rift from the preexisting ridge. The northern boundary is a zone of compression which migrates along with the propagating tip (Engeln and Stein, 1984).

C. Subduction Zones

One major contribution of seismology to the early developments of plate tectonics was the recognition of the Benioff–Wadati zones of intermediate and deep seismicity and their interpretation as cold downgoing slabs, now interpreted as part of the subduction and ultimate recycling of the oceanic plates. The overthrusting geometry in major interplate earthquakes at subduction zones was confirmed early on (Kanamori, 1971a). A number of secondary problems have brought substantial insight into the mechanics of the subduction process, as well as the elastic structure of the lithosphere itself.

Comparison of the rates of seismic moment release over sufficiently long periods of time with those predicted from published plate motions shows strong differences in behavior between various subduction zones (Fig. 22) (Kanamori, 1977). For major subduction events, the task is made easier by the truly gigantic character of the earthquakes (magnitude M_w reaching 9.5) and the usual proximity of at least a few island stations, allowing the three-dimensional mapping of the fault area through the study of directivity and aftershocks.

While certain subduction zones (most notably Chile, Peru and Alaska) show a generally good quantitative agreement between seismicity and predicted plate motion, others (most notably the Marianas, Vanuatu and Tonga) feature a strong seismic deficiency, which can reach several orders of magnitude in the seismic moment release rate (for example, no earthquakes of magnitude 7.5 are known in the Marianas), indicating that most of the subduction in these areas is taken up by *aseismic creep.* Trenches such as Northern Japan and the Kuriles would be of an intermediate character with 50–60% deficiency. As reviewed by Uyeda and Kanamori (1979), the aseismic character of a subduction zone correlates strongly with extensional back-arc tectonics and development of a marginal sea, with a steeper dip of the Benioff slab, with the absence of a flexural bulge and a gravity high seaward of the trench, and with the generally more andesitic character of the arc volcanics.

All these effects can be ascribed to a general decoupling of the two colliding plates, a model confirmed by studies of the rupture process of subduction zone earthquakes. Body-wave modeling is used to retrieve the time history of the seismic source; some events show a simple rupture propagating rapidly and smoothly along the fault, others a complex series of independent ruptures separated in time, possibly triggering one another. These individual seismic sources along the fault plane have been described by Kanamori (1981) as resulting from the failure of zones of increased strength known as "asperities". In general, earthquakes in the more coupled

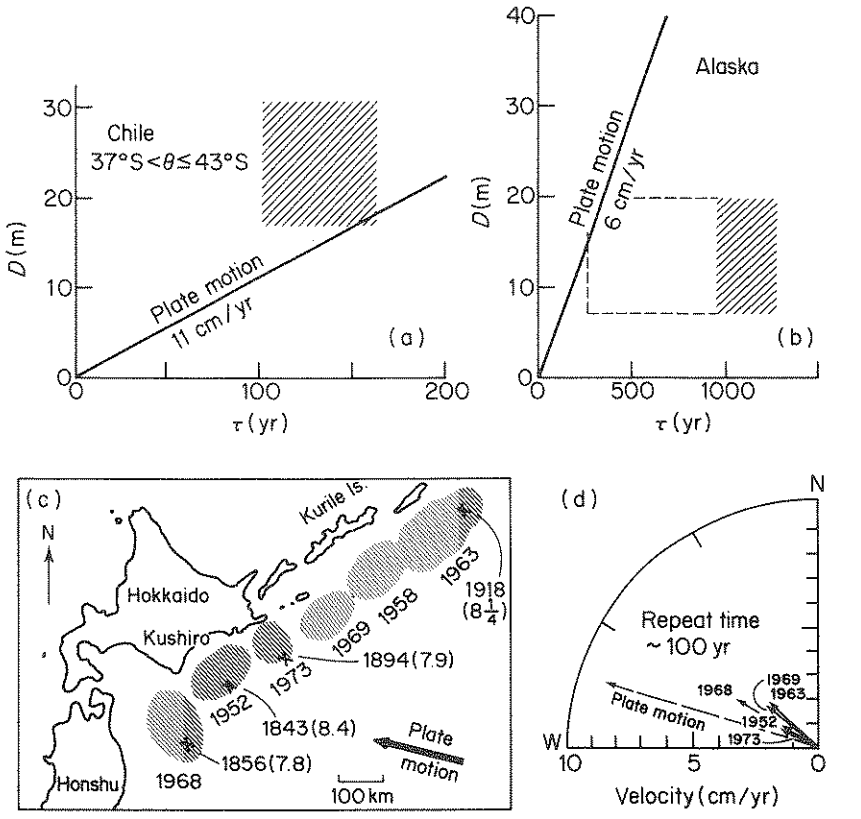

Fig. 22. Comparison of seismic slip and predicted kinematic rates at subduction zones. (a and b): Estimates of seismic slip and recurrence times for large earthquakes (shaded areas), compared with plate motion (line) from Minster and Jordan's (1978) model. Seismic slip located below straight line is deficient and requires aseismic creep. In the case of Alaska (b) [compared to Chile (a)] the dashed box reflects the difficulty of estimating recurrence times (see Kanamori, (1977) for details). (c) Map of the rupture areas of major earthquakes in the Kuriles; arrows represent the direction and rate of seismic slip and plate motion. The seismic slip is clearly deficient by as much as 60% [after Kanamori (1977)].

subduction zones, such as Alaska or Chile, represent the rupture of a single large asperity, whereas earthquakes in partially decoupled areas, such as the Kuriles, involve several distinct asperities (Ruff and Kanamori, 1983). In this interpretation, the areas between asperities yield at lower strains, in the form of foreshocks or aseismically. When the density of asperities becomes very low, they can no longer trigger each other, and seismic events are limited to the rupture of an isolated small asperity, as in the case of the Mariana Trench.

Studies of the maximum known size of earthquakes at subduction zones suggest that the degree of coupling at a trench is a trade-off between the velocity of convergence of the two plates and the age of the subducting lithosphere (Ruff and Kanamori, 1980). On the one hand, a higher collision velocity may favor stronger coupling; on the other hand, the older the subducting plate, the denser it is, and the stronger the *slab-pull* on the plate. This negative buoyancy force tends to sink the subducting plate, and thus may favor decoupling (Fig. 23). Other parameters, such as the development of back-arc spreading and the state of stress in the subducting plate are also controlled by this trade-off. In situations where either a young plate subducts slowly (e.g. Alaska) or an old one subducts fast (e.g. Japan or Tonga), local compressional stresses in the plate can give rise to double Benioff zones (Fujita and Kanamori, 1981; Kawakatsu, 1985).

Seaward of the trench, constraints on the mechanical state of the lithosphere can be obtained from the study of intraplate earthquakes identified by Stauder (1968) as due to the bending of the plate. Later, Chen and Forsyth (1978) identified a pattern of tensional faulting in the upper part of the plate (to a depth of 25 km) and thrusting in its lower part (between 40 and 50 km). Chapple and Forsyth (1979) and Bodine *et al.* (1981) use rheological models with an upper elastic layer and a lower plastic layer to fit the observed depth distribution of flexural events (Fig. 24).

Occasionally, the trench areas are the sites of great earthquakes featuring normal faulting (e.g. Sanriku, 1933, $M_w = 8.4$; Peru, 1970, $M_w = 7.9$; Indonesia, 1977, $M_w = 8.3$). There has been some controversy as to whether to interpret these earthquakes as bending events in the framework of Chen and Forsyth's (1978) "upper" earthquakes or as rupture and decoupling of the entire lithosphere under slab pull. The shallow centroid depth and very fast moment release of the 1977 Indonesian earthquake (Silver and Jordan, 1983) both favor the bending model; on the other hand, for the 1933 Sanriku event, Kanamori (1971b) has argued that a fault width of 100 km is necessary to account for near-field and tsunami amplitudes. In the singular case of the deeper 1977 Tonga event, both aftershock distribution, and the slower rate of seismic moment release suggest vertical rupture extending possibly over 100 km in depth, favoring the decoupling model (Silver and Jordan, 1983).

V. Localized Intraplate Processes

Frequently, seismicity can be used to identify and study regions where intraplate deformation appears to be controlled by localized causes. Many such cases exist; we discuss a few particularly significant or interesting ones.

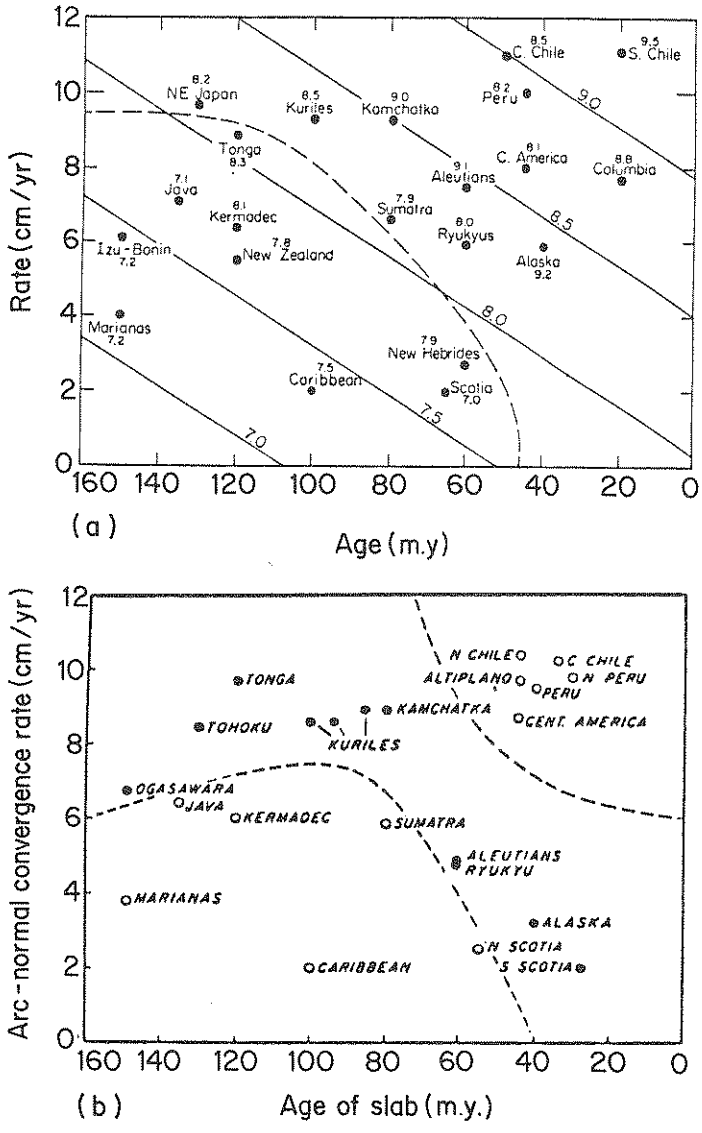

Fig. 23. Variation of coupling at subduction zones as a function of convergence rate and slab age. (a) Maximum known earthquake magnitude M_w. The dashed line outlines the range of back-arc spreading and basin development, and the straight lines are an empirical model for the data [After Ruff and Kanamori, (1980)]. (b) State of stress in the downgoing slab [After Fujita and Kanamori (1981)]. The dashed lines outline the region of compressional stress in which double Benioff zones can exist; ● indicates compressional and ○, tensional stress.

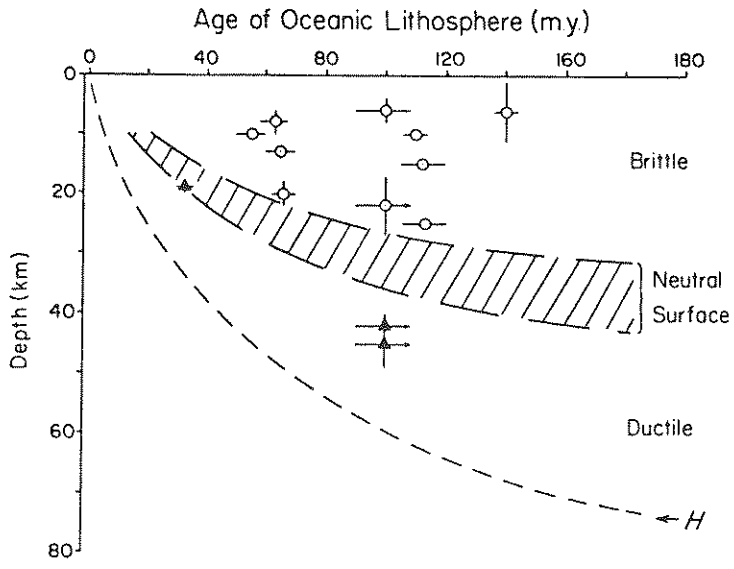

Fig. 24. Focal depths of outer rise flexural earthquakes seaward of trenches (Chapple and Forsyth, 1979) and predictions of a flexural model with a yield strength rheology (Bodine *et al.*, 1981). The plate mechanical thickness H increases with age as expected from thermal models (Figs. 4 and 5). Tensional (○) events occur above the neutral surface while compressional (▲) events occur below.

A. Concentration of Seismicity: Local Stresses or Plate Weakness?

Oceanic intraplate earthquakes occur primarily at sites of preferential seismic release, rather than at random in the plates. Although, in principle, this could be an artifact of the limited time span of instrumental seismology, the occasional occurrence of repeat earthquakes (Okal, 1981) argues against this possibility. The preferential character of intraplate seismic sites has been confirmed in both teleseismic and regional investigations (Okal *et al.*, 1980). The question arising is whether these locations are seismic due to preferential release of platewide stresses at zones of local weakness or due to stress concentrations of local origin. The general correlation of stresses inferred from focal mechanisms over plate-wide distances and the success of simple models of their origin, argue in favor of local weakness. Also, a recent experiment has shown agreement between seismic stress release and the orientation of *in situ* stress measured in a borehole (Newmark *et al.*, 1984). Zones of weakness and preferential seismic release include healed fracture zones (Sykes, 1978), lines of age discontinuity (Okal, 1981) and areas with seamounts and other fossil tectonic features (Stein and Okal,

1978; Okal and Cazenave, 1985). However, their identification is made difficult by our poor knowledge of small-scale bathymetry; also, in at least one case, a detailed shipboard survey has shown no anomalous morphological feature suggestive of weakness at "Region A" in the central Pacific, where 86 earthquakes above magnitude 3.2, generally consistent with ridge-push, were detected in a 15-yr period (Okal *et al.*, 1980).

In some areas of concentrated seismicity on older ocean floor, focal mechanisms clearly incompatible with ridge-push suggest localized regimes of stress, whose interpretation requires a detailed (and often unavailable) knowledge of the bathymetry and tectonics. Such examples include large-scale intraplate deformation (in the Indian Ocean), stresses generated at passive margins, intraplate volcanism and evolving plate boundaries.

B. Large-scale Deformation: The Indian Ocean

The Indian Ocean is characterized by an extraordinary level of intraplate seismicity, as shown by magnitude 7 events near the Ninetyeast and Chagos "aseismic" ridges (Fig. 25). Indian Ocean intraplate seismicity has been studied extensively (Stein and Okal, 1978; Stein, 1978; Bergman *et al.*, 1984; Bergman and Solomon, 1985; Wiens, 1985) but is very poorly understood. Earthquake mechanisms along the Ninetyeast Ridge (which is as active seismically as portions of the San Andreas Fault) are generally consistent with left lateral strike-slip motion, and can be interpreted as resulting from a boundary zone between portions of the plate. Stein and Okal suggested that this relative motion results from the Indian (west) side encountering resistance due to the Himalayan collision, while the Australian (east) side subducts smoothly at the Sumatra Trench. The deformation may be localized as the Ninetyeast Ridge marks the location of a former transform boundary. In stark contrast, the region along the Chagos–Laccadive Ridge shows normal faulting.

The region between the two ridges is seismically active, generally showing thrust and strike-slip faulting and characterized by anomalies in heat flow (Geller *et al.*, 1983), gravity and bathymetry (Weissel *et al.*, 1980). Furthermore, as discussed earlier, the region of young lithosphere in the central Indian Ocean is an unusual zone of normal faulting.

This intraplate deformation is sufficient to provide statistical significance to the modeling of the Indian plate as two plates in inversions of global relative plate motions (Minster and Jordan, 1978; Stein and Gordon, 1984). It is still unclear whether this separation is real, what it implies and how it relates to the variety of deformation styles over the region. Additional relative plate motion data for the area should provide some help. Further

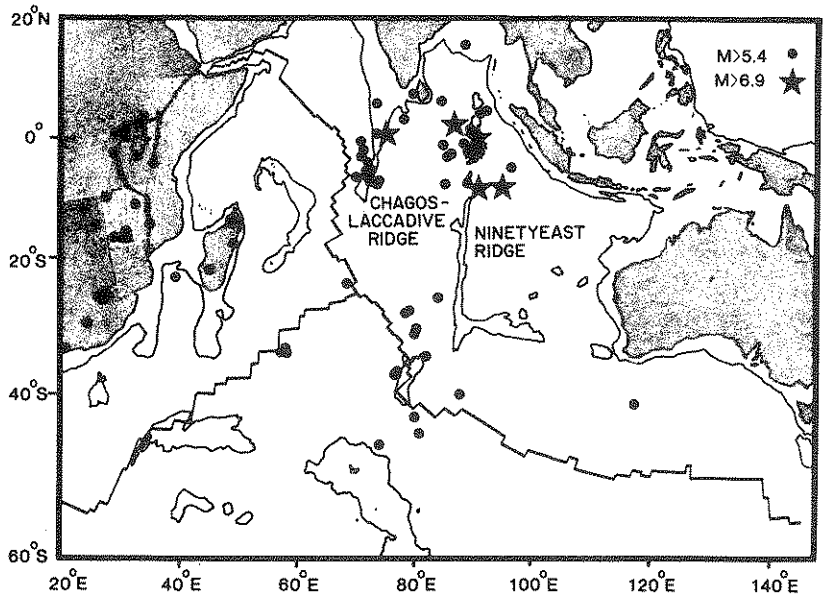

Fig. 25. Intraplate seismicity of the Indian Plate, the most seismically active area of the ocean basins. Magnitude-seven earthquakes occur near the Ninetyeast and Chagos–Laccadive Ridges.

insight may be derived from tectonic models such as the finite element calculation of the theoretical stress field for the Indian Plate (Cloetingh and Wortel, 1985) (Fig. 26). The predicted stresses in the Ninetyeast Ridge area are very large and consistent with the focal mechanisms. Finally, the Indian Ocean example points out the difficulty in distinguishing intense intraplate deformation from a slow (1 cm/yr) plate boundary: the distinction can be rather arbitrary.

C. Seismicity at Passive Margins

An interesting type of intraplate seismicity occurs at passive margins, where continental and oceanic lithosphere join. Although these areas are in general tectonically inactive, major earthquakes can occur. The type example is the active seismic zone on the eastern coast of North America (Stein *et al.*, 1979), which includes the 1929 Grand Banks ($M_s = 7.2$) and 1933 Baffin Bay ($M_s = 7.3$) earthquakes. These events are thought to involve stresses related to the removal of Pleistocene glacial loads extending on to the continental shelf, which reactivated faults remaining from the original

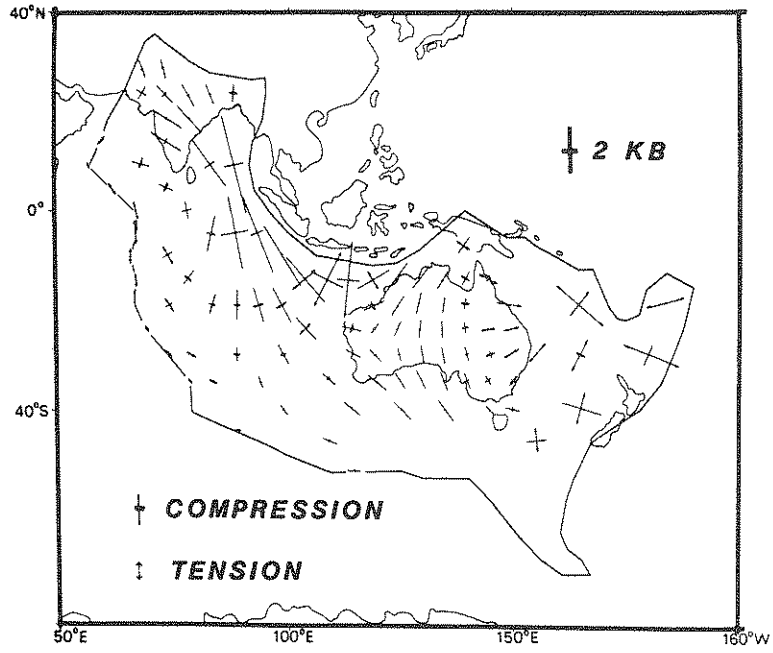

Fig. 26. Theoretical stress model for the Indian Plate (Cloetingh and Wortel, 1985). The predicted high stresses near the Ninetyeast Ridge are consistent with the earthquake focal mechanisms.

rifting. Simple flexure calculations predict stresses of 100–150 bar, adequate to trigger earthquakes (Stein *et al.*, 1979; Quinlan, 1984). While all passive margins are subject to a stress field due to the differing densities of continental and oceanic lithosphere (Bott and Dean, 1972) the effect of deglaciation appears to be to trigger earthquakes, as such events are observed primarily on glaciated margins, such as eastern Canada, Fennoscandia and Greenland.

D. Volcanism

Intraplate volcanism, expressed most spectacularly in the Hawaiian-type island chains, is thought to be a general property of the seafloor (Batiza, 1982). Statistical arguments suggest that it contributes as much as 6% to the total surface of the ocean floor (Jordan *et al.*, 1983). Most of these seamounts are still to be discovered due to poor knowledge of small-scale bathymetry.

In areas of documented volcanism (i.e. reaching above sea level), a clear geographic and often temporal correlation exists between volcanic and

seismic activities, and earthquake mechanisms have been successfully interpreted in the framework of the magmatic evolution of the volcano. Examples include deep fracture under increased magma pressure (Eaton and Murata, 1960), horizontal faulting upon magma intrusion (Furumoto and Kovach, 1979), and post-eruptive caldera collapses (Kaufman and Burdick, 1980). Because of the particular mechanical conditions of the magmatic bodies and surrounding rock, volcanic earthquakes feature several singular characteristics.

Volcanic earthquakes, responding to strain rates as high as 10^{-12}/s, can extend deeper into the lithosphere and have been located under Hawaii down to 55 km (Butler, 1982). In addition, the generally weaker character of the rock leads to rupture at low levels of strain, and preferential concentration of seismicity at lower magnitudes, as confirmed from rock mechanics experiments (Mogi, 1963). Finally, the mechanism of earthquake rupture can depart significantly from the simple model of slip on a fault plane. Significant second double-couples and isotropic sources have been documented in volcanic areas (Dziewonski *et al.*, 1983), and on a much smaller scale, resonant magma oscillation inside cracks leads to high-frequency tremor observed prior to and during volcanic eruptions (Aki and Koyanagi, 1981).

In underwater areas with no record of volcanism, these characteristics have been used to identify and discover active submarine volcanoes [e.g. Macdonald (Norris and Johnson, 1969) and Teahitia (Talandier and Okal, 1984)]. However, recognition of a seismic swarm as volcanic is made difficult by such factors as poor depth control at regional distances and rapid spatial attenuation of tremors. Most importantly, reduced detection capabilities can leave most of a volcanic swarm undetected, with only a few events recorded. Thus, the possibility that a major single earthquake recorded in a remote oceanic area may be part of an unsuspected episode of active volcanism cannot always be discarded, and the interpretation of such an event in terms of large-scale tectonic stresses may be erroneous. For example, Okal (1984) has speculated that a major normal faulting event in 1955, on the flank of Crough Seamount in the east central Pacific, may be related to volcanic activity.

E. Evolving Plate Boundaries

A characteristic of plate boundary systems is often their stability over extended periods of time; e.g. the Mid-Atlantic Ridge has kept an approximately constant orientation and spreading rate for the past 160 Ma. There exist however cases when plate boundaries *must* change, primarily because of

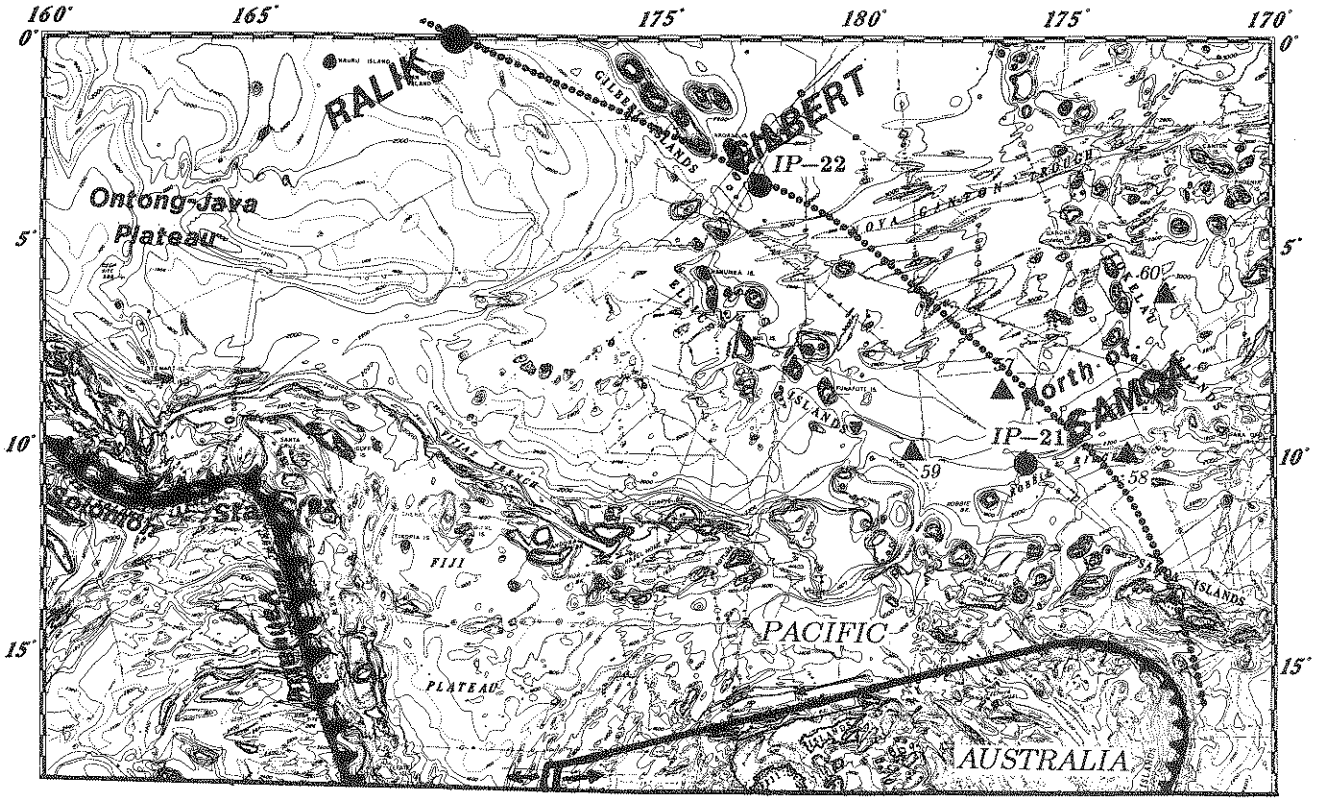

Fig. 27. Map of the Ralik–Gilbert–Samoa Island area, with intraplate seismicity [individual dots and triangles; see Okal (1984)]. The dotted line indicates the potential new plate boundary.

the unsubductible character of continents and of very young oceanic lithosphere. A well-known example is the cessation of subduction at the western edge of North America in the Eocene (Atwater, 1970). The process involved in the reorganization of the plate system is a complex one, which can feature the transient existence of a number of platelets (Menard, 1978). One such platelet is believed to be the Caroline Plate, northwest of New Guinea, where subduction under the Australian Plate has ceased (Kaplan and Seno, 1982). Seismicity in the Caroline Plate is characterized by comparatively deep earthquakes (down to 28 km at only 40 Ma), and generally north-south compressional stresses. Both features can be due to underthrusting of the Pacific Plate under the Caroline Plate, possibly accompanied by shortening (Weissel and Anderson, 1978; Wiens and Stein, 1983).

Another region of interest is the area extending north of Samoa to the Gilbert Islands and beyond, where at least three seismic foci have been identified (see Fig. 27) (Lay and Okal, 1983; Okal, 1984; Walker, 1984). Focal mechanisms at the Gilbert site require a horizontal compressional stress oriented N20°E, more or less at right angles to ridge-push, and clearly of a regional nature. One possible explanation would interpret the Samoa-Gilbert-Ralik seismic line as an incipient subduction zone, which in the future will take up the convergence between the Pacific and Australian Plates: the present subduction system at the Vanuatu (ex-New Hebrides), Santa Cruz and South Solomon Trenches is about to collide with buoyant structures such as New Caledonia, the Norfolk and d'Entrecasteaux Ridges and the Loyalty and Rennell Islands, All this material is light and cannot subduct and the same applies to the overthrusting material on the Pacific side (Fiji and Ontong-Java plateaus), barring a simple reversal of the polarity of the subduction. Thus, the subduction zone will have to jump in search of subductible material, possibly along the Samoa-Ralik seismic line. Although speculative, this interpretation explains the compressional nature of the Gilbert events, and predicts an eventual and general realignment of the southern boundary of the Pacific Plate to the north of the unsubductible material making up the Caroline Plate and the Ontong-Java and Fiji Plateaus.

Acknowledgments

The research effort of the authors described in this review was supported by NSF grants EAR 84-07510, EAR 82-06381 (SS), and EAR 81-06106 (EAO), under ONR Contracts N-00014-79-C-0292 and N-00014-84-C-0616 (EAO), NASA Crustal Dynamics Contract NAS5-27238 (SS) and a Cotrell Research Grant (SS). Acknowledgment is made to the donors of the Petroleum Research Fund, administered by the American Chemical Society, for partial support of this research (SS).

References

Aki, K. and Koyanagi, R. Y. (1981). *J. Geophys. Res.* **86**, 7095–7109.

Aki, K. and Richards, P. G. (1980). "Quantitative Seismology", 2 Vols., Freeman, San Francisco, California.

Artyushkov, E. V. (1973). *J. Geophys. Res.* **78**, 7675–7708.

Anderson, R. N., Forsyth, D. W., Molnar, P. and Mammerickx, J. (1974). *Earth Planet. Sci. Lett.* **24**, 188–202.

Atwater, T. (1970). *Geol. Soc. Am. Bull.* **81**, 3513–3536.

Batiza, R. (1982). *Earth Planet. Sci. Lett.* **60**, 195–206.

Bergman, E. A. and Solomon, S. C. (1980). *J. Geophys. Res.* **85**, 5389–5410.

Bergman, E. A. and Solomon, S. C. (1984). *J. Geophys. Res.* **89**, 11415–11441.

Bergman, E. A. and Solomon, S. C. (1985). *Phys. Earth Planet. Int.* **40**, 1–23.

Bergman, E. A., Nábělek, J. L. and Solomon, S. C. (1984). *J. Geophys. Res.* **89**, 2425–2443.

Bodine, J. H., Steckler, M. S. and Watts, A. B. (1981). *J. Geophys. Res.* **86**, 3695–3707.

Bonatti, E. (1978). *Earth Planet. Sci. Lett.* **37**, 369–379.

Bott, M. H. P. and Dean, D. S. (1972). *Nature* **235**, 23–25.

Brace, W. F. and Kohlstedt, D. L. (1980). *J. Geophys. Res.* **85**, 6248–6252.

Bratt, S. R., Bergman, E. A. and Solomon, S. C. (1985). *J. Geophys. Res.* **90**, 10249–10260.

Burr, N. C. and Solomon, S. C. (1978). *J. Geophys. Res.* **83**, 1193–1205.

Butler, R. G. (1982). *Geophys. J. R. Astron. Soc.* **69**, 173–186.

Cande, S. C., Herron, E. M. and Hall, B. R. (1982). *Earth Planet. Sci. Lett.* **57**, 63–74.

Cathles, L. M. (1975). "The Viscosity of the Earth's Mantle," Princeton Univ. Press, Princeton, New Jersey.

Chapple, W. M. and Forsyth, D. W. (1979). *J. Geophys. Res.* **84**, 6729–6749.

Chase, C. G. (1978). *Earth Planet. Sci. Lett.* **37**, 355–368.

Chen, T. and Forsyth, D. W. (1978). *J. Geophys. Res.* **83**, 4995–5004.

Chen, W.-P. and Molnar, P. (1983). *J. Geophys. Res.* **88**, 4183–4214.

Cloetingh, S. and Wortel, W. (1985). *Geophys. Res. Lett.* **12**, 77–80.

Cox, A. V. ed. (1973). "Plate Tectonics and Geomagnetic Reversals," Freeman, San Francisco, California.

Dziewonski, A. M., Friedman, A., Giardini, D. and Woodhouse, J. H. (1983). *Phys. Earth Planet Int.* **33**, 76–90.

Eaton, J. P. and Murata, K. J. (1960). *Science* **132**, 925–938.

Engeln, J. F. and Stein, S. (1984). *Earth Planet Sci. Lett.* **68**, 259–270.

Engeln, J. F., Wiens, D. A. and Stein, S. (1986). *J. Geophys. Res.* **91**, 548–577.

Fleitout, L. and Froidevaux, C. (1983). *Tectonics* **2**, 315–324.

Forsyth, D. W. (1972), *Earth Planet. Sci. Lett.* **17**, 189–193.

Forsyth, D. W. (1973). *Nature* **243**, 78–79.

Forsyth, D. W. (1975). *Geophys. J. R. Astron. Soc.* **43**, 103–162.

Forsyth, D. W. and Uyeda, S. (1975). *Geophys. J. R. Astron. Soc.* **43**, 163–200.

Forsyth, D. W. and Wilson, B. (1984). *Earth Planet. Sci. Lett.* **70**, 355–362.

Fox, P. J. and Gallo. D. G. (1984). *Tectonophysics* **104**, 205–242.

Fujita, K. and Kanamori, H. (1981). *Geophys. J. R. Astron. Soc.* **66**, 131–156.

Fujita, K. and Sleep, N. H. (1978). *Tectonophysics* **50**, 207–221.

Fukao, K. (1970). *Bull. Earthquake Res. Inst. Univ. Tokyo* **48**, 707–727.

Furumoto, A. S. and Kovach, R. L. (1979). *Phys. Earth Planet. Int.* **18**, 197–208.

Geller, C. A., Weissel, J. K. and Anderson, R. N. (1983). *J. Geophys. Res.* **88**, 1018–1032.

Hager, B. H. and O'Connell, R. J. (1979). *J. Geophys. Res.* **84**, 1031–1048.

Handschumacher, D. W., Pilger, R. H., Jr., Forman, J. A. and Campbell, J. F. (1981). *Geol. Soc. Am. Mem.* **154**, 63–76.
Herron, E. M. (1972). *Nature* **240**, 35–37.
Hey, R. N. (1977). *Earth Planet. Sci. Lett.* **37**, 321–325.
Jordan, T. H., Menard, H. W. and Smith, D. K. (1983). *J. Geophys. Res.* **88**, 10508–10518.
Kanamori, H. (1971a). *Tectonophysics* **12**, 187–198.
Kanamori, H. (1971b). *Phys. Earth Planet. Int.* **4**, 289–300.
Kanamori, H. (1977). *In* "Island Arcs, Deep Sea Trenches and Back Arc Basins" (M. Talwani and W. C. Pitman, III, eds.) pp. 163–174. Maurice Ewing Series, 1. Am. Geophys. Un., Washington, D.C.
Kaplan, D. A. and Seno, T. (1982). *EOS, Trans. Am. Geophys. Un.* **63**, 1023 (abstract).
Kaufman, K. and Burdick, L. J. (1980). *Bull. Seismol. Soc. Am.* **70**, 1759–1770.
Kawakatsu, H. (1985). *Nature* **316**, 53–55.
Kirby, S. H. (1980). *J. Geophys. Res.* **85**, 6353–6363.
Kroeger, G. C. and Geller, R. J. (1986). *J. Geophys. Res.* (in press).
Lachenbruch, A. H. and Sass, J. H. (1980). *J. Geophys. Res.* **85**, 6185–6223.
Langston, C. A. and Helmberger, D. V. (1975). *Geophys. J. R. Astron. Soc.* **42**, 117–130.
Lay, T. and Okal, E. A. (1983). *Phys. Earth Planet. Int.* **33**, 284–303.
Lister, C. R. B. (1975). *Nature* **257**, 663–665.
Macdonald, K. C. and Fox, P. J. (1983). *Nature* **302**, 55–58.
Mammerickx, J., Herron, E. M. and Dorman, L. M. (1980). *Geol. Soc. Am. Bull.* **91**, 263–271.
McKenzie, D. P. (1967). *J. Geophys. Res.* **72**, 6261–6273.
Menard, H. W. (1978). *J. Geology* **86**, 99–110.
Menard, H. W. and Atwater, T. (1968). *Nature* **219**, 463–467.
Mendiguren, J. A. and Richter, F. M. (1978). *Phys. Earth Planet. Int.* **16**, 318–326.
Minster, J. B. and Jordan, T. H. (1978). *J. Geophys. Res.* **83**, 5331–5354.
Mogi, K. (1963). *Bull. Earthq. Res. Inst. Univ. Tokyo* **41**, 615–658.
Naar, D. F. and Hey, R. N. (1986). *J. Geophys. Res.* **91**, 3425–3438.
Newmark, R. L., Zoback, M. D. and Anderson, R. N. (1984). *Nature* **311**, 424–428.
Norris, R. A. and Johnson, R. H. (1969). *J. Geophys. Res.* **74**, 650–664.
Okal, E. A. (1981). *Earth Planet. Sci. Lett.* **52**, 397–409.
Okal, E. A. (1984). *J. Geophys. Res.* **89**, 10053–10071.
Okal, E. A. and Cazenave, A. (1985). *Earth Planet Sci. Lett.* **72**, 99–116.
Okal, E. A., Talandier, J., Sverdrup, K. A. and Jordan, T. H. (1980). *J. Geophys. Res.* **85**, 6479–6495.
Parsons, B. and Richter, F. M. (1980). *Earth Planet. Sci. Lett.* **51**, 445–450.
Parsons, B. and Sclater, J. G. (1977). *J. Geophys. Res.* **82**, 803–827.
Peltier, W. R. (1980). Physics of the Earth's interior. *Proc. Int. Sch. Phys.* "*Enrico Fermi*". (A. M. Dziewonski and E. Boschi, eds.), pp. 362–431. North-Holland, Amsterdam.
Peltier, W. R. (1983). *Nature* **304**, 434–436.
Quinlan, G. (1984). *Can. J. Earth Sci.* **21**, 1018–1023.
Richter, F. M. (1977). *Tectonophysics* **38**, 61–88.
Richter, F. M. and McKenzie, D. P. (1978). *J. Geophys.* **44**, 441–471.
Ruff, L. J. and Kanamori, H. (1980). *Phys. Earth Planet. Int.* **23**, 240–252.
Ruff, L. J. and Kanamori, H. (1983). *Phys. Earth Planet. Int.* **31**, 202–230.
Sclater, J. G. and Fisher, R. L. (1974). *Geol. Soc. Am. Bull.* **85**, 683–702.
Silver, P. G. and Jordan, T. H. (1983). *J. Geophys. Res.* **88**, 3273–3293.
Sleep, N. H. and Rosendahl, B. R. (1979). *J. Geophys. Res.* **84**, 6831–6839.
Solomon, S. C. and Burr, N. C. (1979), *Tectonophysics* **55**, 107–126.
Stauder, W. J. (1968). *J. Geophys. Res.* **73**, 7693–7701.

Stein, S. (1978). *Geophys. J. R. Astron. Soc.* **55**, 577–588.
Stein, S. and Gordon, R. G. (1984). *Earth Planet. Sci. Lett.* **69**, 401–412.
Stein, S. and Okal, E. A. (1978). *J. Geophys. Res.* **83**, 2233–2245.
Stein, S., Sleep, N. H., Geller, R. J., Wang, S.-C. and Kroeger, G. C. (1979). *Geophys. Res. Lett.* **6**, 537–540.
Sykes, L. R. (1967). *J. Geophys. Res.* **72**, 2131–2153.
Sykes, L. R. (1978). *Rev. Geophys. Space Phys.* **16**, 621–688.
Sykes, L. R. and Sbar, M. L. (1974). In "Geodynamics of Iceland and the North Atlantic area" (L. Kristjansson, ed.) pp. 207–224. Reidel Publ., Boston, Massachusetts.
Talandier, J. and Okal, E. A. (1984). *J. Geophys. Res.* **89**, 11216–11234.
Turcotte, D. L. and Oxburgh, E. R. (1967). *J. Fluid Mech.* **28**, 29–42.
Turcotte, D. L. and Oxburgh, E. R. (1973). *Nature* **244**, 337–339.
Uyeda, S. and Kanamori, H. (1979). *J. Geophys. Res.* **84**, 1049–1061.
Walker, D. A. (1984). *OPA, Newsletter of the Ocean P Alliance*, Univ. Hawaii, Honolulu, 15 November 1984.
Weissel, J. K. and Anderson, R. N. (1978). *Earth Planet. Sci. Lett.* **41**, 143–158.
Weissel, J. K., Anderson, R. N. and Geller, C. A. (1980). *Nature* **287**, 284–291.
Wiens, D. A. (1985). *Earth Planet. Sci. Lett.* **76**, 350–360.
Wiens, D. A. and Stein, S. (1983). *J. Geophys. Res.* **88**, 6455–6468.
Wiens, D. A. and Stein, S. (1984). *J. Geophys. Res.* **89**, 11442–11464.
Wiens, D. A. and Stein, S. (1985). *Tectonophysics* **116**, 143–162.
Wilson, J. T. (1965). *Nature* **207**, 343–347.
Yu, G.-K. and Mitchell, B. J. (1979). *Geophys. J. R. Astron. Soc.* **57**, 311–341.